Escuela de
Ingeniería y Arquitectura
Universidad Zaragoza

Trabajo Fin de Máster
Máster Universitario en Ingeniería Electrónica
Curso 2016/2017

Diseño e implementación de una red inalámbrica de sensores para monitorización y comunicaciones en túneles

Samuel Barrios Valero

Director: José Luis Villarroel Salcedo

Departamento de Informática e Ingeniería de Sistemas
Escuela de Ingeniería y Arquitectura
Universidad de Zaragoza

Septiembre 2017

Mi agradecimiento a José Luis Villarroel por su ayuda y orientación en la tarea de dirección de este proyecto y a todos los compañeros de laboratorio, con especial mención a Danilo Tardioli, por su atenta e inestimable colaboración en todo momento.

Resumen

Este trabajo aborda el desarrollo de una red inalámbrica de sensores autónomos capaz de monitorizar un túnel. El punto de partida es la investigación realizada por el grupo de Robótica, Percepción y Tiempo Real (RoPeRT) de la Universidad de Zaragoza en propagación de la señal de radiofrecuencia en entornos tipo túnel. En base a estudios previos se realiza un análisis experimental en el Túnel ferroviario de Somport, con el objetivo de planificar un despliegue de los nodos de la red aprovechando la propagación particular en este tipo de entornos, dando lugar a una topología de red tipo cadena.

A continuación, se implementa un protocolo de comunicaciones multi salto sobre IEEE 802.15.4, permitiendo una gestión energética eficiente de los nodos de la red. De esta forma, los dispositivos se mantienen en un modo de bajo consumo, interrumpiéndolo periódicamente para tomar medidas del entorno y comunicarlas a un nodo base situado en la boca del túnel. Este procedimiento requiere de una sincronización precisa, necesaria para que todos los nodos coincidan durante ventanas temporales periódicas, obtenida mediante la aplicación de *Duty-Cycle Synchronization*.

Finalmente, se demuestra la capacidad de la red como infraestructura de comunicaciones pese al bajo ancho de banda de IEEE 802.15.4. Así, se implementa la teleoperación de un robot móvil, el cual envía mediante la red las lecturas de un LIDAR, recibiendo comandos de movimiento procedentes de un joystick. De esta forma se emula una situación de emergencia, determinada por la lectura de un valor anómalo por parte de un nodo, en la que se introduce el robot en el túnel para inspeccionar la zona.

Abstract

This work addresses the development of a wireless network of autonomous sensors capable of monitoring a tunnel. The starting point is the research carried out by the Robotics, Perception and Real Time (RoPeRT) group of the University of Zaragoza regarding radio frequency signal propagation in tunnel-like environments. Based on previous studies, an experimental analysis is carried out in the Somport Railway Tunnel, with the aim of planning a deployment of network nodes taking advantage of the particular propagation in this type of environment, giving rise to a chain-type topology.

Then, a multihop communication protocol is implemented over IEEE 802.15.4, allowing an efficient energy management of the network nodes. In this way, the devices are kept in a low-power mode, waking them up periodically to perform environmental measurements and communicate them to a base node at the tunnel entrance. This procedure requires a precise synchronization, necessary for all nodes to coincide during periodic temporary windows, obtained by applying Duty-Cycle Synchronization.

Finally, the capacity of the network as a communications infrastructure is demonstrated despite the low bandwidth of IEEE 802.15.4. This way, a mobile robot teleoperation is implemented, which sends the readings of a LIDAR through the network, receiving movement commands from a joystick. This emulates an emergency situation, triggered by the reading of an anomalous value by a node, in which the robot is introduced into the tunnel to inspect the area.

TRABAJOS DE FIN DE GRADO / FIN DE MÁSTER

Escuela de Ingeniería y Arquitectura Universidad Zaragoza

DECLARACIÓN DE AUTORÍA Y ORIGINALIDAD

(Este documento debe acompañar al Trabajo Fin de Grado (TFG)/Trabajo Fin de Máster (TFM) cuando sea depositado para su evaluación).

D./Dª. Samuel Barrios Valero,

con nº de DNI 17768565F en aplicación de lo dispuesto en el art. 14 (Derechos de autor) del Acuerdo de 11 de septiembre de 2014, del Consejo de Gobierno, por el que se aprueba el Reglamento de los TFG y TFM de la Universidad de Zaragoza,

Declaro que el presente Trabajo de Fin de (Grado/Máster) Máster, (Título del Trabajo) Diseño e implementación de una red inalámbrica de sensores para monitorización y comunicaciones en túneles,

es de mi autoría y es original, no habiéndose utilizado fuente sin ser citada debidamente.

Zaragoza, 18 de septiembre de 2017

Fdo: 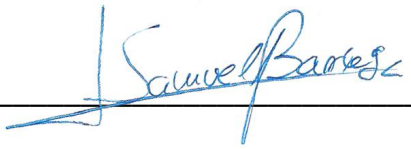

Contents

List of Figures

List of Tables

Chapter 1

Introduction

1.1 Motivation

The construction of different infrastructures, such as roads or railways, faces the challenge of saving multiple geographic accidents. A frequent solution in many of these cases is the construction of tunnels. However, building underground and digging tunnels are processes under an inherent risk. For this reason, this kind of works are carried out with intense security campaigns, geological studies, and high safety protocols.

Nevertheless, the dangerous nature of the tunnel does not end after its construction. Once in operation, it is common for vehicles to accumulate indoors, emitting harmful gases in a confined environment. This, together with a fire, can lead to major disasters, resulting in the death of many people. For this reason, in recent years a lot of work has been dedicated to the development of security systems for this type of environment, being promoted by the issuance of regulations such as the European Directive 2004/54/EC.

Within these security systems, a distinction can be made between detection and actuation systems. The former are focused on tunnel monitoring in order to identify potential hazards. Conversely, the latter take action once the danger occurs, minimizing the possible consequences.

Regarding monitoring systems, numerous works have been carried out. However, these systems are usually generic wired or wireless sensor networks, implemented in the tunnel without addressing or taking advantage of the characteristics of this environment. In addition, in many situations the energy consumption of the network is not taken into account, since the tunnels usually present power cables capable of supplying electricity to the infrastructure.

As example of wireless implementations, [1] develops a fire alarm system for tunnels, capable of collecting real-time data of temperature, smoke and toxic gases and transmitting the measurements combining wireless communication free band and General Packet Radio Service (GPRS). A Wireless Sensor Network (WSN) is developed in [2] to measure the intensity of light in the tunnel and adapt the levels of luminosity of the lamps, communicating the data by IEEE 802.15.4 [3] over 2.4 GHz. Finally, a communication wireless system using ZigBee and WiFi technology is presented in [4], achieving functions of gas monitoring and video surveillance.

In all these works, the propagation of the communications signal and its possible applications are not taken into account. As [5] addresses, radio frequency (RF) propagation in tunnels can be modeled in the same way as the propagation of radio waves in a waveguide. As a result, this environment allows to achieve much higher ranges than those obtained outdoors, allowing the same coverage range with a lower number of nodes. However, this is not a fully beneficial situation, since this propagation results in periodic signal fadings, which can compromise the integrity of the communications system.

One of the objectives of this work is the study of RF signal propagation in tunnel-like environments, as well as its possible application in the nodes deployment of a wireless sensor network. In this way, by avoiding positioning in the fading zones, it is possible to optimize the energy consumption of the nodes, obtaining a greater effective range for the same emission power.

Following the pursuit of energy efficiency in the system, the next step is the development of an operating protocol that minimizes power consumption. In this way, a strategy is implemented in which the nodes are in a low-energy mode, waking up periodically to take measurements of the environment and communicate them to a node at the entrance of the tunnel (gateway). For this purpose, a low power and bandwidth protocol such as IEEE 802.15.4 is used, implementing a strategy of synchronization and multihop communication.

Finally, the use of the system as an emergency communications infrastructure is proposed. This is emulated by means of a scouting mission in which a mobile robot is teleoperated from the base, located at the tunnel entrance. Through a lossy compression strategy, smooth teleoperation is made possible despite the low bandwidth of the network.

The results of the experimental campaign in the Somport Railway Tunnel, the node deployment study and the robot teleoperation strategy are presented in the *ROBOT'2017: Third Iberian Robotics Conference* [6] (attached in Appendix B).

1.2 Structure of the Work

Following the introduction, Chapter 2 deals with RF signal propagation in tunnel-like environments. It includes the theoretical analysis, the experimental campaign in the Somport Railway Tunnel and the node deployment strategy. Next, Chapter 3 introduces the problems given by nodes' clock inaccuracies and develops a method to synchronize the network, allowing to keep the nodes in a low-energy mode and awakening them periodically in order to sense and save energy. Chapter 4 addresses the mobile robot teleoperation, where a proof of concept experiment is performed. Finally Chapter 5 forms the conclusions.

Chapter 2

RF Signal Propagation in Tunnels and Nodes Deployment

2.1 Introduction

Wireless communication systems have become increasingly important as they represent, most of the time, a faster, more economical, and sometimes the only option to deploy a network, as in the case involving mobile agents. A huge effort has been made in terms of mathematical modeling and measuring campaigns in order to predict radio-wave propagation in different types of scenarios, from indoor, outdoor, urban to even underground, with the final goal of ensuring a good quality communication link and increasing the channel's capacity.

Among these scenarios, tunnels have attracted the attention for train applications, vehicular networks, and even service and surveillance missions in both military and civilian contexts [7–11]. Wireless propagation in these environments is described as strongly multipath, and if the wavelength of the signal is much smaller than the tunnel cross section they act as an oversized dielectric waveguide, extending the communication range but affecting the signal with strong fadings [12, 13].

The analysis of the propagation of electromagnetic waves inside a tunnel with arbitrary cross section is not analytically feasible. Even for simple geometries, such as rectangular or circular cross section, no exact closed form solutions are available. To obtain approximate solutions, the most common approaches are the Modal Theory, taking into consideration the interaction between the propagating modes [12, 14–16], and the Geometrical Optics Theory (such as the Ray Tracing approach), which models radio

signals as rays [17–21]. A survey about radio propagation modeling in these scenarios is presented in [22].

It is of special interest the influence of the operating frequency, the antenna characteristics, the tunnel cross section geometry and its longitudinal uniformity. As an example, [23] presents a complete analysis of propagation in tunnels and mines focusing on the effects of the operating frequency and antenna polarization, while [24] studies the influence of the tunnel geometry, and [25] considers the case of tunnels with varying cross section.

In the literature the presence of strong fadings is highlighted, but only the ones that take place in the longitudinal dimension have received attention. In [12, 16, 26], the authors provide approximate mathematical expressions for propagation considering the tunnel as an oversized dielectric waveguide with circular or rectangular geometry, making emphasis on the longitudinal fadings phenomena. However, the signal also suffers from strong fadings in the cross-sectional dimension of the tunnel, resulting in a three-dimensional structure.

The objective of this chapter is to study the RF signal propagation in tunnels, establishing the field both in the longitudinal and transverse dimensions and therefore the 3D structure of fadings. Knowing the fadings position it is possible to use it to develop a deployment of the WSN nodes, obtaining a greater coverage and avoiding problems in communications. This way, the next step is to carry out a study of the link based on the RSSI. Thus, a deployment of nodes in a chain-type topology is developed, optimizing the number of devices needed to cover the tunnel extension.

Objectives are first addressed through theoretical analysis. This allows to establish the necessary knowledge base, as well as to plan a more complete experimental analysis. Through the latter, a measurement campaign is carried out in the Somport Railway Tunnel, achieving a characterization of signal propagation and a deployment of nodes.

2.2 Theoretical Analysis

In this work the Modal Theory approach has been adopted, using the expressions for the electromagnetic field modes and the corresponding propagation constants obtained by [26] for rectangular hollow dielectric waveguides, that are valid for high enough frequencies (i.e. with free space wavelength much smaller than the tunnel cross section dimensions). These solutions are called hybrid modes because both the electric and magnetic field have non-null longitudinal component, although both are much smaller than transversal ones.

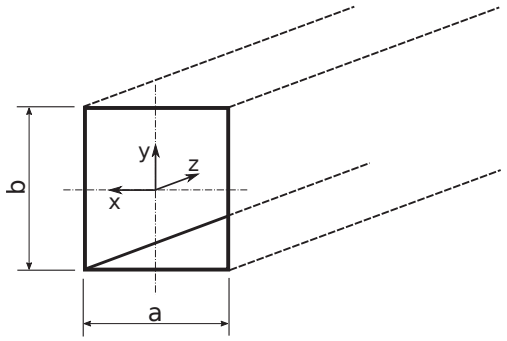

Figure 2.1: Rectangular tunnel coordinate system.

A Cartesian system is placed at the tunnel center (Fig. 2.1). The plane $z = 0$ contains the transmitting antenna (tx), that in our case will be a vertically oriented dipole. Further inside the tunnel ($z > 0$), vertically oriented dipoles will be the receiving antennas (rx).

The electromagnetic field excited by an antenna inside a tunnel can be described as a superposition of different propagating modes associated with the guiding characteristics of the tunnel. The power coupled to each mode depends on the antenna type and polarization, and also on its orientation and position inside the tunnel.

An emitting antenna radiating P_{tx} total power at a frequency f is modeled as an ideal vertical half wave dipole with its center located at coordinates $(x_{tx}, y_{xt}, z_{tx} = 0)$. It is assumed a sinusoidal filament current distribution along its length

$$I_{tx}(y) = I_0 \cos[k_0(y - y_{tx})] \,, \tag{2.1}$$

where

$$I_0 = \sqrt{\frac{2P_{tx}}{73}} \tag{2.2}$$

and

$$k_0 = \lambda = \frac{c}{f} \,. \tag{2.3}$$

For this antenna orientation, only the coupling to the EH^y_{mn} modes of the rectangular tunnel is relevant (where m represents the number of half-waves along the x axis and n the number of half-waves along the y axis). To estimate it, we followed a procedure similar to the one outlined in Appendix G of [12] for the EH^x_{11} mode, that we have extended to any EH^y_{mn} mode with the technique described in Chapter 4 of [27] for rectangular metallic waveguides. This is indeed an approximation. The tunnel acts as an oversized dielectric waveguide and thus the tangential electric field on the walls is not null, as it would be the case in the metallic waveguides. But for frequencies high enough to get free space wavelengths much smaller than the tunnel size, the tangential fields for the relevant propagating modes are small enough at the tunnel walls so that the

metallic waveguide boundary conditions are satisfied to a good enough approximation, giving the same mode shapes as the corresponding modes with the same mn indexes in tunnel size metallic waveguides [12]. There is a significant difference, though: as the free space wavelength is much smaller than the tunnel size, the wave impedance of the modes in the tunnel is quite close to the free space one, $\theta_0 \approx 377\,\Omega$. Then, following [27], A^+_{mn}, the amplitude of the EH^y_{mn} mode traveling in $+z$ direction, as:

$$A^+_{mn} = \frac{\eta_0}{ab} \int_{y'=y_{tx}-\lambda_0/4}^{y'=y_{tx}+\lambda_0/4} e_{mn}(x_{tx}, y') I_{tx}(y') dy' \,, \tag{2.4}$$

being e_{mn} the modal electric field (see Eq. (2.10)). To compute the power coupled to a vertical receiving antenna located at coordinates (x, y, z), the y-directed electric field at this position is needed, that is:

$$E^+_y = \sum_{m,n} A^+_{mn} e_{mn}(x, y) e^{-\gamma_{mn} z} \,. \tag{2.5}$$

Where $\gamma_{mn} = \alpha_{mn} + j\dfrac{2\pi}{\lambda_{mn}}$ is the EH^y_{mn} mode propagation constant, as derived in [26]. The sum should extend over all the possible modes, although in practice only a few ones are relevant. Once propagating, every mode decays exponentially with an attenuation constant α_{mn}, that in [16] is well approximated for frequencies with wavelength much smaller than the tunnel dimensions as:

$$\alpha_{mn} \simeq \frac{1}{2}\left(\frac{c}{f}\right)^2 \left[\frac{m^2}{a^3}\frac{1}{\sqrt{\epsilon_r - 1}} + \frac{n^2}{b^3}\frac{\epsilon_r}{\sqrt{\epsilon_r - 1}}\right] \,, \tag{2.6}$$

c being the free space velocity of electromagnetic waves, f the operating frequency, and ϵ_r the relative permittivity. Hence, the attenuation is higher for low frequencies, and higher order modes attenuate faster than lower order ones.

Each mode propagates with its own wavelength λ_{mn} (close but not equal to the free space one), that from Eq. (54) in [16] can be written as:

$$\lambda_{mn} = \frac{\lambda}{1 - \frac{1}{2}\left(\frac{m\lambda}{2a}\right)^2 - \frac{1}{2}\left(\frac{n\lambda}{2b}\right)^2} \,. \tag{2.7}$$

If two modes with different wavelengths (λ_1 and λ_2) are present, the phase delay accumulated by each one will be different for a given travel distance z. The superposition of the modes will take place with different relative phases in different positions inside the guide, producing constructive interference if both modes are in phase and destructive interference if the relative phase differs in π. This gives rise to a periodic fading structure of the RF power inside the waveguide. The period of this fading structure D is the

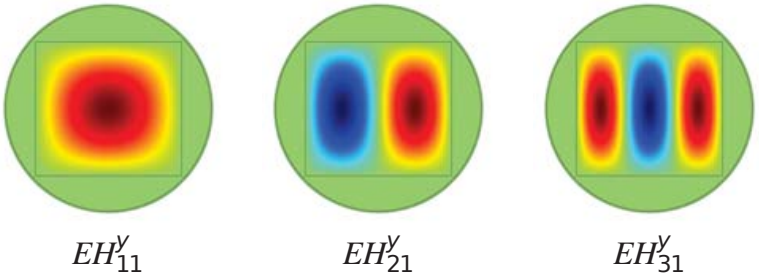

Figure 2.2: Field distribution for the first three modes across a rectangular waveguide section. Red-yellow shades depict positive values, while the blue shades, negative values. Green represents zero field.

distance that creates a relative phase of 2π among the two considered modes:

$$D = \frac{\lambda_1 \lambda_2}{|\lambda_1 - \lambda_2|} \, . \tag{2.8}$$

That for practical purposes, from Eq. 2.7 yields:

$$D = \frac{8}{\frac{c}{f}\left|\frac{m_2^2 - m_1^2}{a^2} + \frac{n_2^2 - n_1^2}{b^2}\right|} \, . \tag{2.9}$$

As the transmitter-receiver setup used in this work benefits the excitation and detection of the EH^y_{m1} modes, notice that only the width of the waveguide determines the period of the fadings.

If more than two propagating modes are present, each possible couple of wavelengths will create its own periodic fadings structure. The total electromagnetic field will be the superposition of all of them.

In the tunnel cross section, for a given z, the electric field of the y-polarized hybrid modes is given by [26]:

$$\begin{aligned} e_{mn}(x,y) = &\left\{\cos\left(\frac{m\pi}{2a}x + \phi_x\right) - \sin\left[\frac{i}{ka\sqrt{\epsilon - 1}}\left(\frac{m\pi}{2a}x\right)\right]\sin\left(\frac{m\pi}{2a}x + \phi_x\right)\right\} \\ &\left\{\sin\left(\frac{n\pi}{2b}y + \phi_y\right) + \sin\left[\frac{i\epsilon}{kb\sqrt{\epsilon - 1}}\left(\frac{n\pi}{2b}y\right)\right]\cos\left(\frac{n\pi}{2b}y + \phi_y\right)\right\} \, , \end{aligned} \tag{2.10}$$

with

$$\phi_x = \frac{1 + (-1)^m \pi}{4} \, , \; \phi_y = \frac{1 + (-1)^n \pi}{4} \, , \tag{2.11}$$

$$k = \frac{2\pi}{\lambda} \, , \tag{2.12}$$

$$\epsilon = \epsilon_r - \frac{i\sigma\epsilon_0}{2\pi f} \, . \tag{2.13}$$

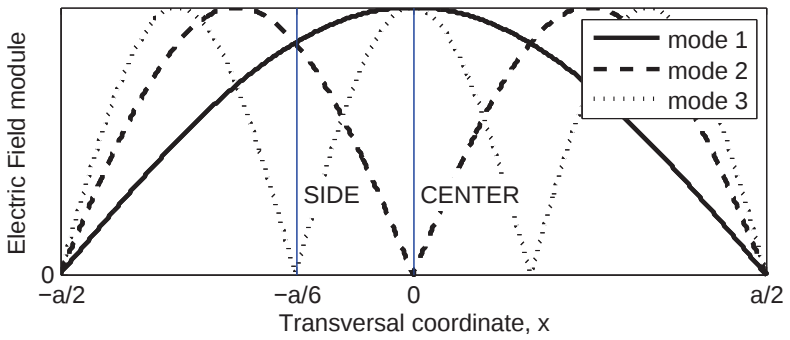

Figure 2.3: Module of the first three modes as a function of the transmitter position along a transversal line at the middle height (y = 0).

As an example, Fig. 2.2 represents the field distribution for the first three EH^y_{m1} modes along a rectangular waveguide cross section (m = 1, 2 and 3) for a fixed z.

The approach adopted in the present paper differs from others such as [28] in a way that instead of placing the transmitting antenna in arbitrary or practical locations (e.g. studying transmitter positions considering the presence of a train), we intend to study location to motivate the appearance of well-shaped periodic fadings (i.e. just two modes interacting) for nodes deployment purposes. To this end, the transversal structure of the modes will be used. Tuning the power coupled to a given mode is accomplished by means of choosing the antenna position in the tunnel cross section (see Eq. (2.4)): close to a point where a given mode has an amplitude maximum (or minimum) to maximize (or minimize) the coupling. As in the far sector only the first two or three lower order modes survive (as suggested by Eq. (2.6) and the experimental results), Fig. 2.3 represents the coupled amplitude of the first three propagating modes along the tunnel cross section for a fixed y. In the figure, two emitter positions are marked out. In the *CENTER* position the emitter generates the EH^y_{11} and EH^y_{31} modes with maximum amplitude, but not the EH^y_{21}. In the *SIDE* position the emitter generates the EH^y_{11} and EH^y_{21} modes with large amplitude, but not the EH^y_{31} mode. These transmitter positions will be used in the sequel sections to promote and analyze fading structures.

It can be seen that at the center of the tunnel (position *CENTER* in Fig. 2.3, $x = 0$), the interaction between the first and third mode takes maximum value, while minimizing the influence of the second mode. In a similar way, positions around one third from the tunnel walls (position *SIDE*, $x = -a/6$) maximize the interaction between the first and second mode, while minimizing the influence of the third mode.

As an example, Fig. 2.4, shows the fadings structure (along x and z dimensions for a fixed y) generated by a transmitter in the *SIDE* position (modes EH^y_{11} and EH^y_{21} interaction).

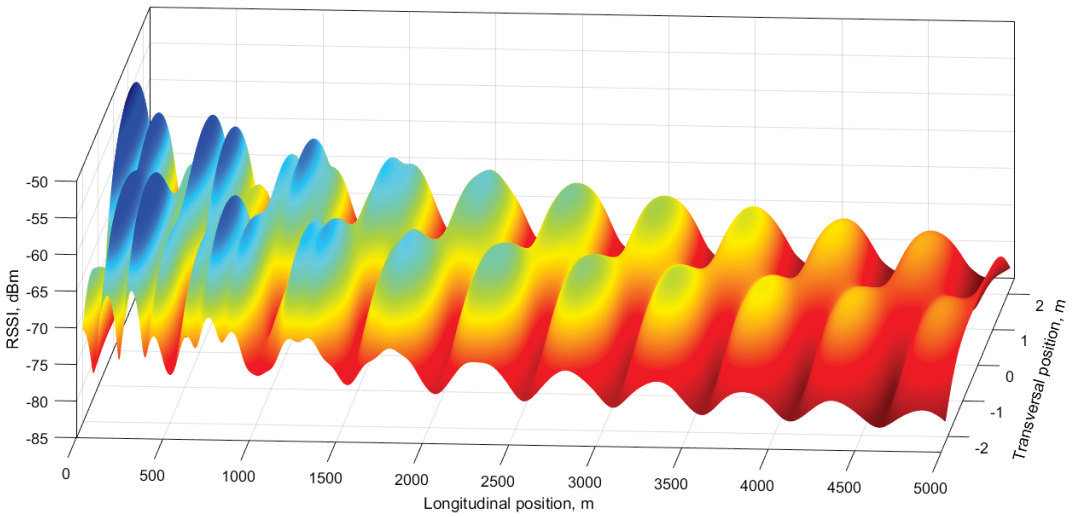

Figure 2.4: Simulated 3D fadings across a rectangular waveguide using the modal theory.

2.3 Scenario and Experimental Setup

2.3.1 The Somport Railway Tunnel

The Somport Railway Tunnel is the chosen location to perform the experiment. It is an out-of-service tunnel which connects Spain and France through the Pyrenees and was used to cover the Pau-Canfranc route until 1970. Nowadays it is an emergency lane for the Somport Road Tunnel and houses the Canfranc Underground Laboratory. It is 7.7 km long and has a horseshoe-shaped section, approximately 5 m high and 4.65 m wide (Fig. 2.5a). The tunnel is straight along its entire length, suffering a change in slope at approximately 4 km from the Spanish entrance. The walls are limestone with short sections covered with a thin concrete layer. The tunnel also has small emergency shelters every 25 m, which are 1 m wide, 1.5 m high and 0.6 m in depth. It has also 17 lateral galleries, which are longer than 100 m and of the same height than the tunnel (Fig. 2.5b). Besides, the Robotics, Perception and Real Time Group (RoPeRT) from the University of Zaragoza has experience in developing work in the tunnel [29]. For these reasons, it is an ideal environment to perform experiments and emulate long tunnels, common in transport or mining applications.

2.3.2 Measurement Setup

As previously mentioned, the behavior of the tunnel as waveguide depends on the signal wavelength being smaller than the transverse dimension of the tunnel. In other words, the higher the signal frequency, the lower the attenuation factor per unit length. An

experimental analysis of the signal propagation in different frequencies of the Industrial, Scientific and Medical (ISM) radio band is performed in [30]. As a result, it is determined that the 2.4 GHz and 5.2 GHz signals have a much lower attenuation factor than those of 433 MHz and 868 MHz. For this reason, 2.4 GHz is the selected frequency band, since it has a high propagation range, a reasonable wall roughness tolerance and a wide variety of hardware available on the market.

Regarding the communications protocol, since one of the objectives of this work is the development of a low energy consumption WSN, IEEE 802.15.4 is the chosen one [3]. This technical standard specifies the physical and media access control layers for Low-Rate Wireless Personal Area Networks (LR-WPANs). It is suitable for communication in networks formed by low cost devices and low transfer rates, up to 250 kbit/s. In addition, the size and frequency of the data to be sensed does not have high bandwidth requirements, so it is possible to discard other protocols with higher transmission rates and energy consumption, such as IEEE 802.11 [31].

According to the described specifications, the chosen radio modules are Digi's XBee 802.15.4 (Fig. 2.6a) and XBee-Pro 802.15.4 (Fig. 2.6b). These devices communicate over IEEE 802.15.4, emitting in a power range of -10 to 0 dBm and 10 to 18 dBm, respectively. They allow a maximum payload of 100 bytes, even tough the maximum size of the 802.15.4 MAC frame is limited to 127 bytes. In addition, they are mounted on XBIB-U-DEV interface boards (Fig. 2.6c), allowing the connection to a computer via USB. Regarding the antennas, Fig. 2.6 shows two different types depending on the module: XBee 802.15.4 uses a whip antenna with a gain of 1.5 dBi. On the other hand, the XBee-Pro 802.15.4 has a 2.1 dBi dipole antenna. Their low price and the fact that

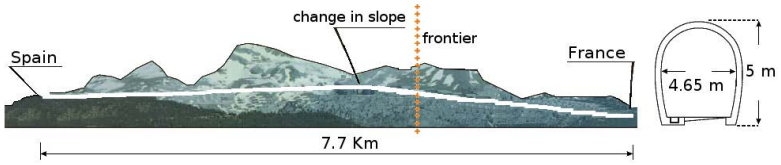

(a) Somport Railway Tunnel

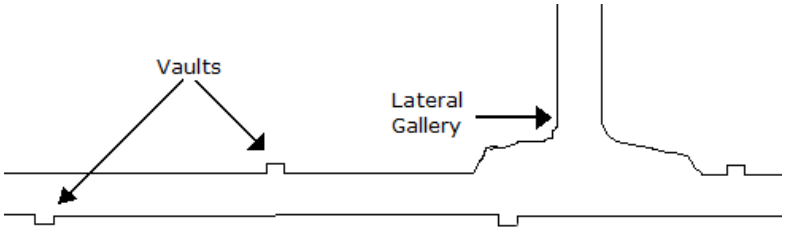

(b) Internal structure of the tunnel

Figure 2.5: Testbed.

(a) XBee 802.15.4 (b) XBee-Pro 802.15.4 (c) XBIB-U-DEV

Figure 2.6: RF modules (a, b) and USB interface board (c).

they can be easily connected to any hardware using USB, make this system suitable for the development of our application.

In relation to the experimental setup, the emitter (Tx) module is placed on a 180 cm tripod separated 160 cm from the wall (Fig. 2.7b). This position is chosen in order to excite the first two modes of the signal, so as to produce better defined and predictable fadings [29], as has been mentioned above. In order to avoid the effect of the change in slope of the tunnel, the emitter is placed close to the highest point of the tunnel, at approximately 4 km from the Spanish entrance (Fig. 2.5a). Hence, it is possible to emulate the change in slope as the joint of two tunnels with different slope, avoiding non-ideal effects.

The selected emission powers are -10, 0 and 18 dBm. The Tx module broadcasts packets of 60 bytes with a numeric identifier, which are captured by an array of two Xbee-Pro 802.15.4 modules, allowing to characterize the influence of transversal fadings, and streaming the data to a computer running ROS (Robot Operating System [32]) over

(a) Instrumented vehicle (b) Emitter module

Figure 2.7: Receiver array on mobile platform (a) and emitter module setup (b).

Ubuntu 14.04. The array modules have a sensitivity of -100 dBm and are at 200 cm height and separated 120 cm apart. As in [33] and [29], the spacing between two successive modules is fixed to be greater than one half of the wavelength, so that the coupling between antennas is minimized.

The receiver array is moved along the tunnel using an off-road vehicle as mobile platform (Fig. 2.7a). In order to synchronize the received packets with the position in the tunnel, it is equipped with two 0.5 degree resolution encoders and a Scanning Laser Rangefinder. The vehicle localizes itself along the tunnel using a localization algorithm on a previously built map [34], allowing to maintain the same position reference for all the experiments. In this way, the periodic emergency shelters every 25 m, characteristic of this testbed, play an important role in the localization and synchronization, allowing to correct the odometric cumulative error after being detected by the laser.

The experiment consists of six sweeps along the tunnel (Table 2.1). For each emission power of the selected set (-10, 0 and 18 dBm), a route is made from the emitter, placed between galleries 8 and 9, moving away until the loss of the signal. At this point, the vehicle returns to the starting point, resulting in two sweeps per power.

2.4 Experimental Results

First, the propagation of the signal is analyzed in the regions near the emitter. The packets have been received by the modules located at the ends of the array (Xbee1 and Xbee2), differentiating between the closest to the emitter side (Tx) and the furthest one, since it is not placed at the center of the tunnel. Fig. 2.8 shows the RSSI of the packets collected during the sweeps 3 and 5. The phenomena of the fadings can be appreciated mainly in the signal received by the closest module to the emitter (Fig. 2.8a). In correspondence with [29], the fadings have a spatial period of about 500 m. Regarding the signal received by the other module, it does not present fadings as sharp as the first one. However, the measured RSSI is enough to ensure a suitable communications link (Fig. 2.8b). Appendix A contains the measured RSSI of the rest of sweeps.

Table 2.1: Parameters of the experiment sweeps.

Sweep	Power (dBm)	Start Gallery	End Gallery	Distance (m)
1	-10	9	6	1510
2	-10	6	9	1484
3	0	9	4	2466
4	0	4	9	2463
5	18	9	1	3777
6	18	1	9	3791

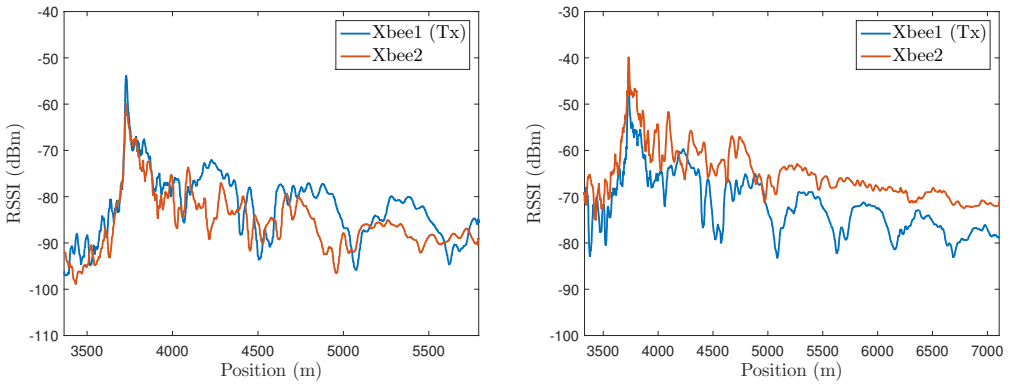

(a) 0 dBm, Galleries 9-4

(b) 18 dBm, Galleries 9-1

Figure 2.8: Fadings measured during the experiment. The closest module to the sending side is indicated by (Tx).

The next step is the measurement of the link quality. The objective is to find a minimum RSSI capable of ensuring the correct communication between two adjacent nodes. The chosen quality estimator is Packet Delivery Ratio (PDR), which is defined as the ratio of the number of packets delivered to the number of packets sent. Since it is a global measure and it is necessary to analyze the PDR during the sweep, a moving average of 20 packets is applied in order to obtain its evolution along the path. Thus, the packets received during the whole experiment are grouped in different ranges according to their RSSI. For each range, the percentage of windows with a PDR equal to 1 is found. This gives a measure of how likely it is that all packets reach their destination for a given RSSI range. Appendix A contains the distribution histograms, while Table 2.2 summarizes the results. It can be observed that for RSSI values higher than -80 dBm the percentage of windows with a maximum PDR is greater than 98%. Depending on the application, it will be necessary to prioritize a greater reliability of packet delivery or to sacrifice it for a greater range of coverage per node. In this work a 98% probability is considered sufficient, which means that each node receives the packets of the adjacent

Table 2.2: Results of the link quality study.

Range (dBm)	No. of Packets	% PDR = 1
[-105, -100)	227	11.31
[-100, -95)	1805	30.93
[-95, -90)	5454	79.17
[-90, -85)	5717	91.81
[-85, -80)	5215	96.56
[-80, -75)	4839	98.68
[-75, -70)	4149	98.84
[-70, -65)	3838	98.98
[-65, -60)	1880	99.73
[-60, -55]	975	100

one with a RSSI higher than -80 dBm. Table 2.3 shows the maximum range achieved during the experiments meeting the minimum RSSI requirement. It can be verified that even for the same power, there are different ranges depending on the module and the path. This is due to the fact that the transverse separation of the receivers to the wall has not been constant during the experiment. Hence, the transversal fadings have a strong influence on the RSSI of the received packets. Therefore, in order to achieve the indicated maximum ranges, a careful positioning of the transverse separation with respect to the emitter must be performed.

Assuming the nodes are placed in the optimal transverse position, the number of devices needed to cover this tunnel (7.7 km) would be 61, 5 and 3, for emission powers of -10, 0 and 18 dBm, respectively. As detailed in following sections, the higher the network size the lower the available bandwidth, which is reduced in a factor $(N-1)$, being N the total number of nodes, since there is not spatial reuse. This is not problematic when monitoring the scenario, because the size of the measured data is usually small, as well as the frequency of sensing. However, a high number of nodes implies a difficulty in establishing a continuous communication, as may be the teleoperation of a robot or a voice call to a user.

Hence, there are two different problems with different requirements that must be addressed separately. First, continuous communication needs the highest coverage range using the least number of nodes. On the other hand, the monitoring of the scenario requires a higher number of nodes emitting with a low power. For this reason, the use of devices with several different emission levels is proposed. In this way, they can work in low power during monitoring situation, where there is not high bandwidth requirement. Besides, in an emergency context, where continuous communication is needed, a minimum number of nodes can raise their power, diminishing the number of hops and providing a higher bandwidth to the network.

Besides, it is necessary to consider that the RSSI is not kept above the minimum desired value during the whole path. Due to the phenomenon of fadings, there are areas where

Table 2.3: Maximum distance where a RSSI of -80 dBm is achieved. Underlined measurements are obtained in the modules next to the sending side.

Sweep	Power (dBm)	Xbee1 Range (m)	Xbee2 Range (m)
1	-10	46	127
2	-10	123	102
3	0	1 557	1013
4	0	379	385
5	18	3 380	3378
6	18	1613	2 780

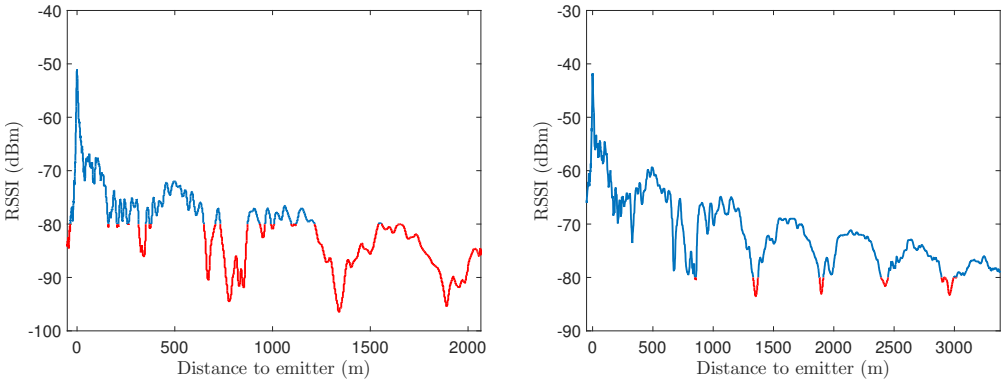

(a) Sweep 3, 0 dBm, Xbee1 (Tx)

(b) Sweep 5, 18 dBm, Xbee1 (Tx)

Figure 2.9: Forbidden regions for the node deployment in the sweeps 3 and 5. Zones where the RSSI is below the minimum required (-80 dBm) are plotted in red while Tx indicates that the module was the closest to the sending side.

the link quality is lower than desired. In this way, forbidden regions are established, where the deployment of a node is not advisable. Fig. 2.9 shows these zones for emission powers of 0 and 18 dBm. In the case of the greater power, it is observed that the zones coincide with the valleys of the fadings, being periodic and predictable. On the other hand, the smaller powers form these regions in higher areas of the fadings, making them comparable in length with the regions suitable for deployment.

Therefore, a simple deployment strategy consists of placing the node $n+1$ in the coverage range of the node n, avoiding the forbidden regions and giving rise to a chain topology. In this way, it is possible to take advantage of the particular signal propagation to obtain an unreachable range in other types of environments. On the other hand, since monitoring applications usually require a periodic separation distance between sensors, a node position may coincide with a forbidden region. In this case, it would be deployed in the closest previous suitable zone, fulfilling the required separation and avoiding the low link quality area.

2.5 Conclusions

In this chapter a nodes deployment strategy has been developed taking advantage of the particular RF signal propagation in tunnel-like environments. Based on a theoretical analysis, the tunnel's behavior as a waveguide has been determined for wavelengths smaller than the tunnel's transverse dimension. This way, a much lower attenuation factor is obtained than in the open field, giving rise to a greater communications coverage. In turn, propagation leads to fading zones, where the RSSI decreases, not being suitable to ensure link quality between nodes.

In order to position these areas and plan a deployment, an experimental analysis has been carried out in the Somport Railway Tunnel. By the use of a transmitter with several emission powers and the displacement of two receivers via an instrumented vehicle, the structure of the fadings was defined. Thus, the minimum RSSI value necessary to ensure communication between two consecutive nodes was found, as well as the zones to avoid in the placement of the devices.

As a result, a node deployment strategy in a chain topology has been developed. Taking into advantage the behaviour of the tunnel as waveguide, the achieved range is optimized with respect to the power consumed by the radio modules of the nodes. This yields in an increase of the network efficiency, reducing the number of nodes necessary to cover a whole tunnel.

Chapter 3

Synchronization and Communication of the WSN

3.1 Introduction

Wireless sensor networks are systems formed by spatially distributed autonomous sensors used to monitor environmental conditions. This kind of tasks requires the coordination of the nodes, since they have to measure with a certain frequency and usually cooperate in order to send the sensed information to a server or a gateway. As mentioned in the previous chapter, this work develops a WSN with chain topology for tunnel monitoring. Hence, only the nearest node can transmit the information directly to the gateway, while the rest must collaborate to communicate the sensed data, resulting in multi-hop communication.

On the other hand, WSNs are composed by autonomous sensors, usually powered by batteries. Even for devices capable of performing harvesting, energy is a very limited resource, which totally conditions the performance of the nodes. For this reason, it is necessary to perform an efficient management of the system, keeping the nodes in sleep mode as long as possible, awakening then periodically to measure and communicate.

However, the implementation of this strategy in wireless networks is not trivial, since it is necessary that all the nodes are awake at the same time to be able to communicate. In wired systems this mode change can be managed by a base-generated interrupt on a bus common to all nodes. Most devices allow to stop the sleep mode by a pin interrupt, which is not possible when the communication is performed by radio. Energy saving in nodes involves turning off the radio modules, isolating them and cutting off any external source of awakening. This way each node is responsible for interrupting its sleep mode

at the right time. For this reason, a synchronization between the nodes that make up the network must be implemented, since it is imperative that everyone matches in a temporary window of activation.

The objective of this chapter is the development of a energy saving strategy, based on keeping the nodes in a sleep mode and waking them up periodically to measure the environment. Through the implementation of a synchronization protocol, it is possible to manage the monitoring through temporary windows, reducing the power consumption of the nodes.

3.2 Clocks Inaccuracies

In WSNs, where each node has its own physical clock, synchronization plays a crucial role in energy saving. Before delving into the details of synchronizing clocks, we define the notion of a clock. A computer clock is an electronic device that counts oscillations in an accurately-machined quartz crystal, at a particular frequency. Computer clocks are essentially timers. The timer counts the oscillations of the crystal, which is associated with a counter register and a holding register. For each oscillation in the crystal, the counter is decremented by one. When the counter becomes zero an interrupt is generated and the counter is reloaded from the holding register. Therefore, it is possible to program a timer to generate an interrupt 60 times a minute, where each interrupt is called a clock tick, by setting an appropriate value in the holding register. At each clock tick, the interrupt procedure increments the clock value stored in memory.

The clock value can be scaled to get the time of the day and the result can be used to timestamp an event on that device. In practice, quartz crystals in each of the nodes

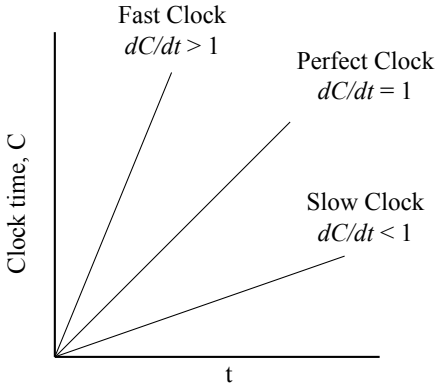

Figure 3.1: Behaviour of fast, slow and perfect clocks with respect to a time reference.

run at slightly different frequencies, causing the clock values to gradually diverge from each other. This divergence is formally called the clock skew, which can lead to an inconsistent notion of time. Thus, clock synchronization is performed to correct this clock skew in WSNs.

The term software clock usually refers to the time in a computer clock to stress that is just a counter that gets incremented by crystal oscillations. The interrupt handler must increment the software clock by one every time an interrupt (i.e., a clock tick) occurs. Most common clock hardware is not very accurate because the frequency that makes time increase is never exactly right. Even a frequency deviation of just 0.001% would cause a clock error of about one second per day. This is also a reason why clock performance is often measured with very fine units like PPM (Parts Per Million) [35].

Consider a system where every node must be synchronized to a reference time. At any point of time, if the reference time is t, the time in the node p is $C_p(t)$. In an ideal world, $C_p(t) = t$ for all p and all t, which means $\frac{dC}{dt} = 1$. However, due to the clock inaccuracy discussed above, a clock is said to be working within its specification if:

$$1 - \rho \leqslant \frac{dC}{dt} \leqslant 1 + \rho \,, \tag{3.1}$$

where ρ is the maximum skew rate specified by the manufacturer. Fig. 3.1 illustrates the behaviour of fast, slow and perfect clocks with respect to a time reference. It is important to note that the value indicated by the manufacturer simply limits the maximum skew of the clock. In practice, this value is highly variable, depending on factors such as temperature, humidity or aging of the device.

The hardware chosen to develop the clock tests is a Raspberry Pi 2 Model B (Fig. 3.2). It is a small and cheap single-board computer with a 900 MHz quad-core ARM Cortex-A7 CPU and 1 GB RAM. Although it is not an ideal hardware for the implementation of sensor networks due to its power consumption, it is suitable for testing, being easy to connect to the XBees through USB. Besides, the embedded Linux allows to remotely

Figure 3.2: Raspberry Pi 2 Model B.

manage the nodes using SSH (Secure SHell), allowing centralized development and testing.

The first step consists of measuring the clock skew among a group of Raspberry Pis. Note that the clock skew value indicated by the manufacturer denotes the deviation of the device from a reliable time reference, given for example by an atomic clock. In our case, the objective is the local synchronization of a group of nodes, being irrelevant its correspondence with a global framework, such as UTC (Coordinated Universal Time). Fig. 3.3 shows the setup, where the time drift of three Raspberry Pis is measured with respect to a time reference given by π_0. Thus, the four devices are connected to a common bus, where π_0 generates a pulse periodically registering its timestamp. This signal triggers a pin interrupt in the slave devices (π_1, π_2 and π_3), storing their timestamp as well. After a running time, it is possible to compare the recorded timestamps, estimating the clock skew between them. In this way, the maximum clock skew measured is 80 PPM approximately, which translates as almost 5 milliseconds per minute or 7 seconds a day. Considering that the time windows during which nodes have to match have a shorter duration than a second, these error rates are unsuitable, requiring the implementation of a synchronization protocol.

3.3 Synchronization Protocol

Synchronization between nodes is usually achieved by the exchange of timestamps and messages, which allows one node to estimate the time of the others clock. Once the time difference is estimated, the nodes can correct or adjust their clock in order to run in tandem. However, the enemy of accurate network time synchronization is the non-determinism of the delay estimation process. Latency computation is disturbed by random events which lead to asymmetric round-trip-message delivery delays [36]. This

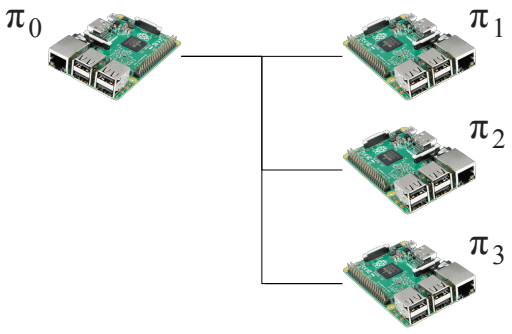

Figure 3.3: Clock skew measurement setup.

contributes directly to synchronization error. In order to understand the source of these errors, [37] proposes the decomposition of a message's latency source in four components:

- Send Time. The time spent at the sender to construct the message. It includes the kernel protocol processing and variable delays introduced by the operating system. Send time also accounts for the time required to transfer the message from the host to its network interface.
- Access Time. Delay incurred waiting for access to the transmit channel. This is specific to the MAC protocol in use. For example, IEEE 802.15.4 implements CSMA/CA (Carrier-Sense Multiple Access with Collision Avoidance), where nodes attempt to avoid collisions by transmitting only when the channel is sensed to be idle.
- Propagation Time. The time needed for the message to transit from sender to receivers once it has left the sender. When the sender and receiver share access to the same physical media, this time is very small as it is simply the physical propagation time of the message through the media.
- Receive Time. Processing time required for the receiver's network interface to receive the message from the channel and notify the host of its arrival. This is typically the time required for the network interface to generate a message reception signal.

Existing time synchronization algorithms differ mainly in their methods of estimating and correcting these sources of error. These methods vary in complexity, from arithmetic averages to linear regressions [38] or statistical distributions [39], also affecting the number of messages exchanged. However, not all of them are suitable for a WSN. It is necessary to consider that these networks are made up of low-cost devices, which sometimes implies low performance, and limited battery life. Besides, the higher the number of messages to exchange, the longer the nodes must stay awake and the lower the energy savings. For this reason, it is advisable to use simple strategies that minimize

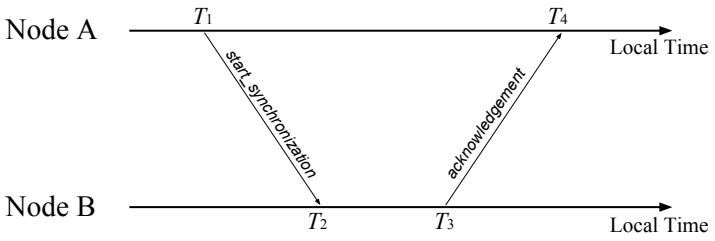

Figure 3.4: Two-way handshake synchronization.

the use of radio and do not require complex operations, such as the two-way handshake implemented in NTP (Network Time Protocol) [40] or TPSN (Timing-sync Protocol for Sensor Networks) [41].

On the other hand, the mentioned protocols are designed for networks without a defined topology, where it may be necessary to discover nearby nodes. For this motive they implement algorithms to order synchronization, such as hierarchical structures. This is not necessary in the designed system, where all nodes are known and their chain topology is fixed. In addition, since the planned deployment in Chapter 2 ensures link quality only between adjacent nodes, a pairwise procedure is a must.

The implemented protocol is based on the mentioned two-way handshake method, used in widely extended protocols such as NTP or TPSN. Consider the message exchange illustrated in Fig. 3.4. At time T_1 (according to its local clock), node A sends a *start_synchronization* packet, which contains the value of T_1, to node B. Node B receives this packet at time $T_2 = T_1 + d + \theta$, where θ and d represent the clock offset between the two nodes A and B, and the propagation delay, respectively. Node B sends back an *acknowledgement* packet to node A at time T_3. This packet carries the values T_1, T_2 and T_3. Then, node A receives the *acknowledgement* message at time T_4. Assuming that the clock offset and the propagation delay is constant in this small span of time, node A can calculate these values by the equation 3.2 and synchronize itself to the clock of node B. This represents a sender-initiated approach, where the sender synchronizes its clock to that of the receiver.

$$\theta = \frac{(T_2 - T_1) - (T_4 - T_3)}{2}, \; d = \frac{(T_2 - T_1) + (T_4 - T_3)}{2} \; . \tag{3.2}$$

This pairwise synchronization can be extended to our chain topology network applying it successively to the links: first, the base node (node 0) broadcasts the *start_synchronization*

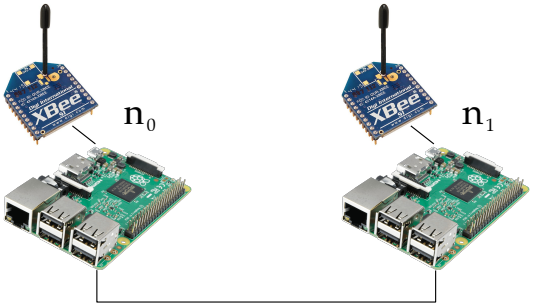

Figure 3.5: Synchronization accuracy measurement setup.

Algorithm 1 Chain Synchronization Protocol

Require:
1: n is the node number, with *0* being the first and N the last.
2: **procedure** SYNC()
3: **if** $n = 0$ **then**
4: *Send start_synchronization to Node 1*
5: *Wait* T_1 *from Node 1*
6: *Send* T_2 *and* T_3 *to Node 1*
7: **end if**
8: **if** $n > 0$ **then**
9: *Wait start_synchronization from Node* $n - 1$
10: *Wait random_time*
11: *Send* T_1 *to Node* $n - 1$
12: *Wait* T_2 *and* T_3 *from Node* $n - 1$
13: *Compute* θ *and* d ▷ [Equation (3.2)]
14: *Adjust clock*
15: **if** $n \neq N$ **then**
16: *Wait* T_1 *from Node* $n + 1$
17: *Send* T_1 *to Node* $n + 1$
18: **end if**
19: **end if**
20: **end procedure**

message. When received by node 1, it starts the two-way handshake with node 0, correcting its clock with the base one. At the beginning of the process, node 2 listens to the emission of the packet containing $T_1 1$ from node 1. Once it receives it, waits for a short-random time (about 100 ms) in order to let the synchronization between nodes 0 and 1 end. Then, it sends its own T_1 to node 1, which is already waiting for the message, beginning the synchronization between them. This process is repeated along the whole network and is summed up in Algorithm 1.

In this way, the network can be synchronized with the clock of the node at the tunnel entrance. It is assumed that this node, which acts as a gateway, is synchronized with a global reference if necessary, transmitting it to the rest of the system by the described method.

Notice that the communication of the synchronization end between two nodes is done implicitly, so that it is not necessary to use an extra message to notify the next one. Thus, the number of messages exchanged is decreased, as well as the use of node radio, reducing energy consumption.

The proposed procedure is designed to be repeated periodically, since during the time that the clocks are running freely they are accumulating an error that must be corrected. In order to characterize the accuracy achieved, the experiment illustrated in Fig. 3.5 is carried out. Two nodes are built using Raspberry Pi and XBee modules, communicated

Table 3.1: Minimum, maximum and average error achieved with the proposed synchronization method for different periods.

T (s)	ϵ_{min} (ms)	ϵ_{max} (ms)	ϵ_{avg} (ms)
60	0,058	2,3	1,1
120	1,2	2,5	1,8
180	1,4	2,3	1,9
300	1,1	3,6	2
3600	1,3	4,5	2,9

via USB. Both have a pin connected to a common bus, so that their clocks are registered as in Fig. 3.3. Then, they are synchronized periodically, studying the error achieved depending on the time between synchronizations, while their clock is recorded. Results are shown in Table 3.1. As can be checked the higher the period, the higher the average error achieved. This is to be expected, since the time between synchronizations the clocks run freely, so the accumulated error increases. With regard to the value achieved for a synchronization per minute, it is suitable for the operation of the system, since it is two orders of magnitude less than waking-up time. However, it is necessary to consider that this value rises with the size of the network, increasing the error as the node is further from the base. This may hinder system operation in the case of using many nodes emitting at low power, since the accumulated error could be significant. In this case it would be necessary to study a different strategy, a more precise error correction or synchronize at a higher frequency.

3.4 Duty-Cycle Synchronization

Based on the work performed in [42], this section integrates the synchronization protocol described above into a Duty-Cycle strategy to reduce energy consumption. In many sensor network applications, such as surveillance or monitoring, nodes are in idle mode for a long time if no sensing event happens. For example, in our system, nodes have the function of taking a measurement of the environment and communicating it to the base. This requires much less time than the sensing frequency, so there is no need for nodes or their radio to be active between measurements. Duty-cycle strategy reduces the listen time by letting the node go into periodic sleep mode. This translates into immediate energy savings. For example, if in each second a node sleeps for half second and listens for the other half, its duty cycle is reduced to 50 %, which leads to energy efficiency close to 50 % (disregarding sleep mode consumption).

The basic schematic is shown in Fig. 3.6. Each node goes to sleep for a while, then wakes up, synchronizes according to the protocol described in the previous section,

takes a measurement of the environment and communicates it to the base. During the sleep, the node turns off its radio, and sets a timer to awake itself later.

The procedure requires periodic synchronization between the nodes, so that their sleeping and waking times coincide. In order to make the system robust to synchronization errors [42] recommends to use a wake-up period significantly longer than clock error or drift. Therefore, the previous pairwise synchronization protocol is integrated into a strategy called SFSB (Synchronize Forwards - Send Backwards). This way, during the *synchronization* phase the system acts as described in Algorithm 1 with a difference: there is a deadline for receiving T_1. Thus, the node waits a limited amount of time for the next node to send its time stamp. If it is not received within the deadline, it assumes that it is either the last node or that the next node has failed or its battery has run out. This check is carried out periodically and influences the next phase. *Communication* is started by the last node to successfully synchronize. It senses the environment, sends this measure to the previous node and goes to sleep. Once the previous node receives the message, it measures and adds the value to the previous one received, sending the set to the following node and sleeping afterwards. It can happen that the number of measures overflows the IEEE 802.15.4 payload. In this case, several messages would be used, reserving a byte in each one to indicate how many are left to arrive. This way, synchronization is initiated at the base, advancing to the end of the network. Once it reaches the last node, it begins sensing and communicating, returning the information to the base.

The main advantage of this strategy is that it makes it possible to detect failures in nodes and prevent their drop from affecting the overall operation of the network. Although the nodes after the fallen one remain isolated, the previous ones continue to function keeping the subnet active.

On the other hand, the main drawback is that tasks are not equally distributed across the network: since the flow begins at the base node and advances, bouncing at the end of the network, the first nodes must wait longer for information to return. For example, in a network of 20 nodes the second one has to wait for another 18 nodes to synchronize and communicate the measurement, while the second last one only has to wait for the last two nodes. This leads to a heterogeneous battery life of the nodes, being shorter in the devices closest to the entrance.

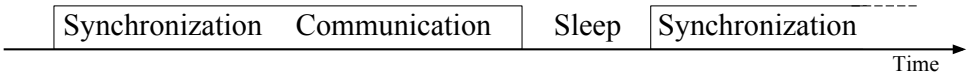

Figure 3.6: Periodic operation of duty-cycle synchronization.

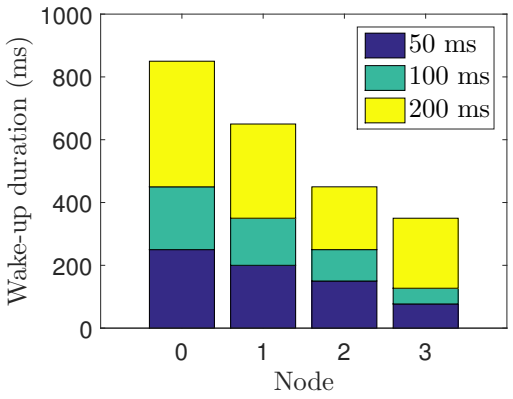

Figure 3.7: Wake-up duration depending on the *random_delay* value in a setup of 4 nodes.

Finally, the *random_delay* value in Algorithm 1 has a direct influence on the time during which the nodes are awake. In order to characterize this impact, an experiment is carried out with a setup of four nodes in which the duration of time awake is measured according to the *random_delay* value.

As can be checked in Fig. 3.7, the lower the node number, the longer it has to stay awake. The value of this duration is estimated as

$$T = 50\,ms + d \times N\ , \tag{3.3}$$

being T the wake-up time, d the value of *random_delay* and N the total number of nodes. For this reason it is essential to use the minimum possible *random_delay* value, since it directly affects the wake-up duration and consumption of the node. On the other hand, it can be seen how, as the number of nodes in the network increases, the consumption of the first nodes increases, as well as the difference in duration between them.

3.5 Power Consumption

According to the chosen hardware, a node is composed of a Raspberry Pi and an XBee module. The manufacturer of the first one indicates a consumption of 420 mA and 260 mA in normal and sleep/idle modes, respectively, feeding at 5 V. This results in 2.1 W and 1.3 W. On the other hand, the consumption of the XBee module depends on the transmitting power. Emitting at 0 dBm, the consumption is 45 mA, while at 18 dBm it amounts to 340 mA, resulting in 148.5 mW and 1.12 W, feeding at 3.3 V. Finally, in idle mode it consumes a maximum of 10 µA, giving rise to 33 µW. Thus, in the case of not employing any energy saving strategy, the total consumption of a node would be 2.25 W and 3.22 W, emitting at 0 dBm and 18 dBm, respectively.

Table 3.2: Power consumed in the least efficient node for different network sizes and transmission powers. The subscript of P indicates the emission power in dBm.

N	D (%)	P_0 (W)	P_{18} (W)
4	0.42	1.304	1.308
10	0.92	1.309	1.318
20	1.75	1.317	1.334
30	2.58	1.325	1.350
50	4.25	1.340	1.382

On the other hand, energy savings depend on the sensing rate required in the installation. The duty-cycle is given by the ratio between the time the node is awake relative to the sensing period. Since the variables measured in a tunnel, such as temperature or gases, have slow dynamics, a measurement every minute is considered a sufficient frequency. Taking into account that the wake-up time is not homogeneous in our system, the worst case duty-cycle D is given by:

$$D = \frac{d \times N + 50\,ms}{1/f} = \frac{50\,ms \times N + 50\,ms}{60}\ . \tag{3.4}$$

Where d is the *random_delay* value, N is the total number of nodes and f is the sensing frequency. Thus, the power consumed by the node is

$$P = P_{ON} \times D + P_{IDLE} \times (1 - D)\ , \tag{3.5}$$

being P_{ON} and P_{IDLE} the power used during normal and idle modes, respectively.

Table 3.2 shows the power consumption in the least efficient node for different transmission powers and network sizes, using 50 ms as *random_value*. It can be checked how, despite the increase in the number of nodes, the consumption is very similar to that of the system in idle mode (1.3 W).

Finally, it must be noted that even 1.3 W is a too high consumption for an autonomous node. However, the hardware has been chosen not for its high efficiency, but for its ease for development. There is specific WSN hardware available on the market with much lower idle-mode consumption, where implementing this strategy results in even greater node battery duration.

3.6 Conclusions

In this chapter the synchronization issues of a chain topology wireless sensor network have been addressed. Starting from a study of the causes and consequences of inaccuracies in nodes' clocks, a synchronization protocol has been developed. This method extends the pairwise procedure of others, such as TPSN or NTP, to a chain network. In this way, the entire system is synchronized with the clock of the tunnel entrance node, which acts as a gateway.

Synchronization allows, in addition to more precise monitoring and greater reliability of sensed information, the implementation of energy saving strategies. An example of this is the Duty-Cycle synchronization developed in the SFSB strategy. Keeping the nodes in a low-power mode and waking them periodically, it is possible to monitor the environment while minimizing the energy consumption of the devices. The solution has been experimentally evaluated, revealing that sensing the environment every minute with this strategy results in a power consumption in the most unfavourable node almost identical to that of the sleep mode, maximizing the nodes' battery life.

Chapter 4

Teleoperation of a Mobile Robot over a Low-Bandwidth Infrastructure

4.1 Introduction

In previous chapters, a wireless sensor network has been developed using IEEE 802.15.4 over a 2.4 GHz RF signal. As mentioned above, the main advantage of this protocol is its low consumption, obtained mainly exchanging information at a low rate. Compared to other widely extended protocols, its bandwidth is relatively poor, achieving a maximum of 250 kbps compared to the tens of Mbps obtained by IEEE 802.11 (WiFi).

This bandwidth limitation is not a problem when developing a monitoring system, since the data obtained from the sensors is usually a few bytes in size. In addition, the sensing frequency is not high, meaning a very light load on the network.

However, since the designed system is able to alert of emergency situations, it is interesting to equip it with an inspection tool. In this way, this work proposes the option that, in a toxic gas emission or fire situation, a teleoperated robot inspects the tunnel until the source is found. In this case, the network would abandon the duty-cycle strategy and remain permanently active, serving as a communications infrastructure for the robot.

This operation would be simple in a communications network with a high bandwidth, capable of supporting the robot's remote operation. However, this is not the case, where the scarce low bandwidth available is reduced as repeaters are used. In this way, the capacity of the network decreases as the robot advances, communicating through an

Figure 4.1: Pioneer P3DX with a LIDAR mounted on top of it.

even deeper node. For this reason, it is necessary to carry out a lossy compression of information.

This chapter shows the results of a proof of concept experiment in which a robot teleoperation is performed over a backbone network made of XBee nodes. The goal is to control the movement of a Pioneer P3DX robot (Fig. 4.1) using a joystick while receiving LIDAR (LIght Detection And Ranging) reading feedback.

4.2 Experimental Setup

The proposed scenario is shown in Fig. 4.2: a Pioneer P3DX mobile robot is teleoperated using a network formed by several XBees acting as repeaters. The robot sends the LIDAR scans through the last node, receiving movement commands from a joystick in the base. Similarly, a laptop sends the motion orders to the first node, receiving the information read by the LIDAR.

The system is built on top of ROS (Robotics Operating System) [32]. It is a robotics middleware which provides services designed for heterogeneous computer clusters such as

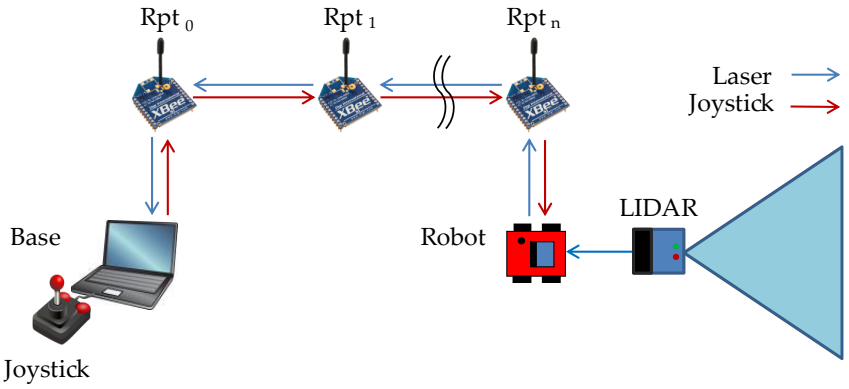

Figure 4.2: Teleoperation schematic.

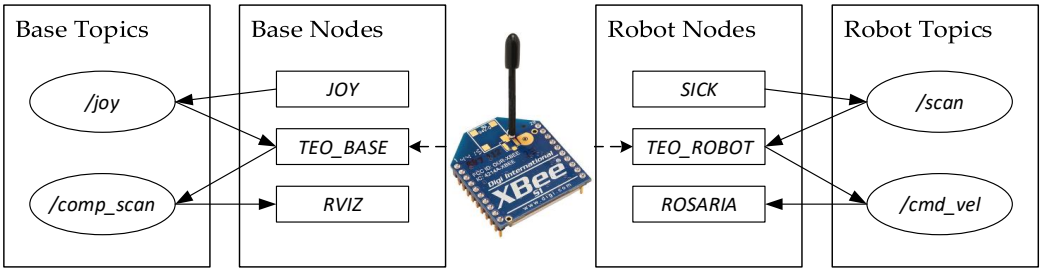

Figure 4.3: ROS nodes and topics involved in the system.

hardware abstraction, low-level device control, implementation of commonly used functionality, message-passing between processes, and package management. It is based on a graph architecture where the processing takes place in the nodes that can receive, send and multiplex sensor, control, status, planning and actuators messages, among others. Messages are routed via a transport system (topic) with publish/subscribe semantics. A node sends out a message by publishing it to a given topic. On the other hand, a node that is interested in a certain kind of data will subscribe to the appropriate topic. There may be multiple concurrent publishers and subscribers for a single topic, and a single node may publish and/or subscribe to multiple topics.

In Fig. 4.3 it is possible to observe the conceptual design of the system: the *JOY* node connected with the joystick publishes the stick movements messages through the */joy* topic; it is read by the *TEO_BASE* node that serializes the information and sends it over the network. On the other side, the messages are received and deserialized by the *TEO_ROBOT* node and published on the */cmd_vel* topic that, in turn, is read by the *ROSARIA* node, which is in charge of sending the velocity commands to the robot microcontroller via RS-232.

In the other direction the LIDAR readings are published by the *SICK* node on the */scan* topic and read by the *TEO_ROBOT* node that, again, serializes the data before sending it over the network. On the base station side, it is deserialized by *TEO_BASE* and published in the */comp_scan* topic to be shown by the *RVIZ* node. Rviz is a 3D visualization tool for ROS which interprets the LIDAR information, plotting a point cloud. In this way the joystick operator is able to identify obstacles and openings, allowing the navigation of the robot. Finally, notice that the nodes on the two ends do not share any *roscore* since each of them consists in a independent ROS system connected through a non-ROS network. Thus, they share in a periodic and asynchronous way the information about the LIDAR and joystick readings.

4.3 Adapting to the Available Bandwidth

Although the theoretical bandwidth of the XBee modules is 250 kbps, the maximum measured experimentally is only 32.5 kbps, due to the bottleneck that their serial port communication introduce. Additionally, the use of repeaters in a network reduces the raw bandwidth by a factor of $1/(N-1)$, being N the total number of nodes. Considering the case of the Somport Railway Tunnel, emitting at the maximum power would require the use of three nodes in order to cover its whole length, which would suppose a bandwidth of 16 kbps. On the other hand, in the case of 10 dBm, the resulting bandwidth would be 8 kbps, since five nodes would be required.

As described, the system is conceptually very simple but being the bandwidth so limited, it is necessary to reduce the information sent in order to be able to obtain an acceptable loop rate. For example, the *SICK* node configured as in the experiment (and connected via serial port to the computer) produces 180 range readings (one per degree) at a frequency of 4 Hz. This corresponds, taking also into account the additional data published (timestamp, maximum and minimum range, etc.), to approximately 0.8 KB of data, 4 times per second that is, 3.2 KB/s. Since the maximum payload of the XBee modules is 100 bytes, sending the raw data would imply splitting the LIDAR message in at least 8 parts and then merge them at the receiver side to rebuild it. This has two implications: on the one hand sending 8 different messages over a network would take several milliseconds (especially over a multi-hop one) reducing the loop rate. On the other hand, the loss of a single message would mean being unable to reconstruct the information. A similar consideration can be made with the joystick commands, even if in this case the information fits in a single packet. Additionally, the more the bandwidth used for these tasks, the less bandwidth available for others. To mitigate this problem, the data is compressed as described below.

4.4 Data Compression

Having high precision and resolution data is usually indicative of a correct system performance. However, if the bandwidth is limited it might not be possible or convenient. Since this is the case, it is decided to reduce the information sent to the minimum necessary to find the data themselves useful. To do so, the precision and the resolution of the data is decreased, maintaining a more than acceptable level. Specifically, the ranges representation is reduced from *float64* (8 bytes) to a single byte of information. The length of each reading is thus scaled to 256 possible values and the maximum range is reduced to 4 m independently on the actual range of the LIDAR sensor. All the values

Table 4.1: Packet Delivery Ratio (PDR) and Inter-Arrival Time (IAT) measured during the experiment. Full indicates the percentage of laser packets recomposed using their two halves, while μ and σ denote mean and standard deviation, respectively.

Source	PDR (%)	Full (%)	μ IAT (ms)	σ IAT (ms)
LIDAR	100	76.6	207	80
Joystick	91	-	282	105

above that are assigned the out-of-range value of *0xFF*. This provides an accuracy of 4 m/254 = 1.5 cm, only 0.5 cm worse than that of the Hokuyo URG-04LX, just to give an example, and more that enough for a teleoperation task where the maximum speed of the robot is limited (0.5 m/s in the experiment).

However, even with this reduction, the whole laser scan does not fit in a single packet (at least 180 bytes are needed, and the maximum payload is 100 bytes), so it is split in 2 halves, using 1 byte as identifier. In order to avoid losing all the information in case one of the two packets does not reach the destination, the first packet contains the even laser readings (0°, 2°, etc.) while the second has the odd ones. If a message cannot be completed with the second part or only the second part is received, the message is published anyway filling the missing information with the *out-of-range* value. In this way it is possible to have a valuable feedback information also in lossy networks.

4.5 Real-World Testing

In order to demonstrate the correct functioning of the system, the following experiment is proposed. Given a room with two doors communicated externally by a corridor, the goal is to teleoperate the robot, making it exit through one and return by the other using only

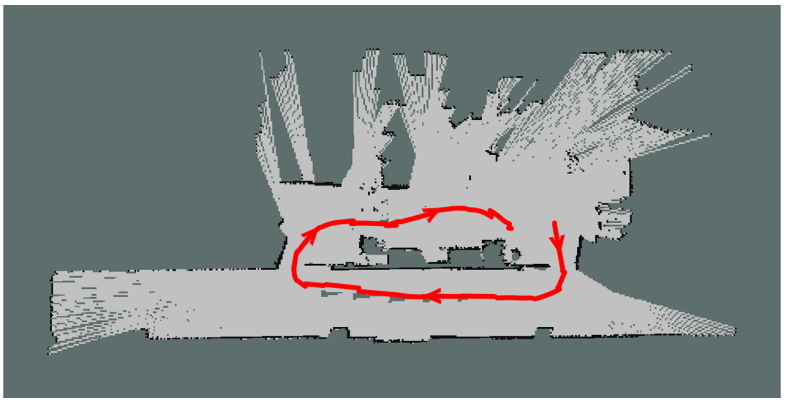

Figure 4.4: Results of the teleoperation experiment. The red line indicates the path followed by the robot.

the visual LIDAR feedback to perform the task. Both the LIDAR and joystick data were sent every 200 ms which is fast enough for an effective teleoperation, while this period allows leaving free bandwidth for other possible flows. The information is sent through a network formed by four XBee modules. Fig. 4.4 shows the path achieved, where the map has been generated using a SLAM (Simultaneous Localization And Mapping) node running in the robot itself while Table 4.1 shows the results in terms of inter-arrival time and PDR for each flow. It can be seen how the packet division strategy achieves that, even though the two halves are not always received, the initial data can be recomposed, resulting in an effective PDR of 100%. As can be checked, it was possible to teleoperate the Pioneer P3DX, which is 40 cm wide approximately, through a door of comparable size.

4.6 Conclusions

In this chapter we have proposed the use of the developed WSN as an emergency backbone network to provide communication to a mobile robot with the end of teleoperating it for on-site intervention. The proposed architecture consists of a network formed by several nodes acting as repeaters. The robot sends LIDAR scans through the last node, receiving movement commands from a joystick in the base. In exchange, a laptop sends the motion orders to the first node, receiving the information read by the LIDAR.

Due to the low-bandwidth available, a lossy compression strategy has been implemented. The size of the LIDAR data has been diminished as well as split in several packages. This way it is possible to teleoperate the robot through the backbone network despite of the bandwidth reduction each repeater adds.

In order to evaluate the system, an emulation experiment was carried out. The objective was to teleoperate a mobile robot using a backbone network of four nodes through comparable size doors. Both LIDAR and joystick data was sent every 200 ms, leaving free band for other possible flows. The path was smoothly achieved, validating the proposed solution.

The real-world experiment demonstrated that such teleoperation is possible allowing a remote operator to explore the environment with the sole LIDAR feedback. These results has given rise to the development of a more complex system, including roaming among the different nodes so that it can be implemented in the tunnel.

Chapter 5

Conclusions

In this work we have developed a low energy consumption wireless sensor network for tunnel monitoring. The energy efficiency is mainly achieved using two strategies: a planned node deployment which takes advantage of the RF signal propagation in tunnels, and a Duty-Cycle synchronization, which keeps the nodes in a low-power mode, waking them up periodically to perform and communicate measurements.

The node deployment deals with the tunnel's behaviour as a waveguide for signals with wavelengths smaller than its transverse dimension. This causes a much lower attenuation factor than in open field, which allows to achieve a greater communication coverage for the same emission power. In exchange, propagation leads to fading zones, where the RSSI decreases, not being suitable to ensure communication between nodes. In order to characterize and locate these areas, an experimental campaign was carried out. This way, a minimum RSSI was obtained to guarantee a quality link between nodes, as well as to avoid areas where this value is not reached. As a result, a node deployment strategy in chain topology has been developed. Taking into advantage the RF signal propagation, the power consumed by the nodes' radio is optimized, decreasing the energy required to cover the whole length of the tunnel.

Duty-Cycle synchronization is achieved by extending pairwise synchronization methods to a chain topology network. Starting from the study of the sources and problems caused by the clock inaccuracies of the nodes, a synchronization protocol was developed. It achieved to synchronize the whole chain network to the time reference given by the node placed at the entrance of the tunnel, given rise to periodic waking-up procedures. The developed SFSB strategy keeps the network node in a low-power mode, interrupting it periodically in order to take and communicate measurements of the environment. This yields into considerable energy savings. In the experimental tests carried out, it has been proved that measuring every minute results at the most unfavourable node in

consumption levels practically identical to those of the sleep mode. These tests have been performed with devices not optimized for WSN, so it is estimated that the savings can be increased using specific hardware.

Finally, the monitoring system is provided with an emergency on-site intervention method. It involves the teleoperation of a mobile robot, which would be able to navigate the tunnel if a node alerted of a dangerous measurement. The proposed architecture consisted of a laptop sending motion commands from a joystick to the robot, which returns LIDAR scans. They communicate through the first and last node, respectively, leaving the rest of devices the role of repeaters. Given the size of the LIDAR data and the low bandwidth available, it was not possible to send raw laser scans as often as necessary. For this reason, a lossy compression was carried out, entailing a reduction and split of the LIDAR data. The solution was tested in a proof of concept experiment in which the robot was teleoperated using a 4 nodes network. The proposed path was achieved smoothly, sending joystick and LIDAR data every 200 ms.

To summarize, we have developed and implemented a low energy consumption WSN using a node deployment strategy based on RF signal propagation and Duty-Cycle synchronization. Besides, an emergency intervention method has been proposed where a teleoperation of a mobile robot is performed. The effectiveness of the solutions has been demonstrated with experiments and a publication in an international conference.

Future Work

It has been demonstrated that the developed system allows energy savings in the network nodes, achieved both with its deployment and waking-up management. However, the results obtained worsen as the number of network nodes increases. In particular, for a large number of devices, the synchronization protocol accumulates a considerable error, which can compromise the correct operation of the network. For this reason it is necessary to develop more complex strategies, involving more accurate error estimations or changes in network topology.

Regarding robot teleoperation, the success of the proof-of-concept gives rise to the development of roaming strategies between nodes. In this way it would be possible to operate the robot throughout the tunnel, changing the communications node as it advances. However, as with synchronization, it is necessary to solve the problems caused by an increase in network size, due to its direct influence on the available bandwidth.

Appendix A

Somport Experiment Results

This appendix contains the results of the experimental campaign carried out in the Somport Railway Tunnel.

Fig. A.1 shows the RSSI measured during different sweeps, distinguishing between the receiver closest to the transmitter wall and the furthest one. On the other hand, Fig. A.2 includes the histograms with the distribution of PDR obtained depending on the RSSI. By combining these two measures, it was possible to design the deployment of the nodes along the tunnel.

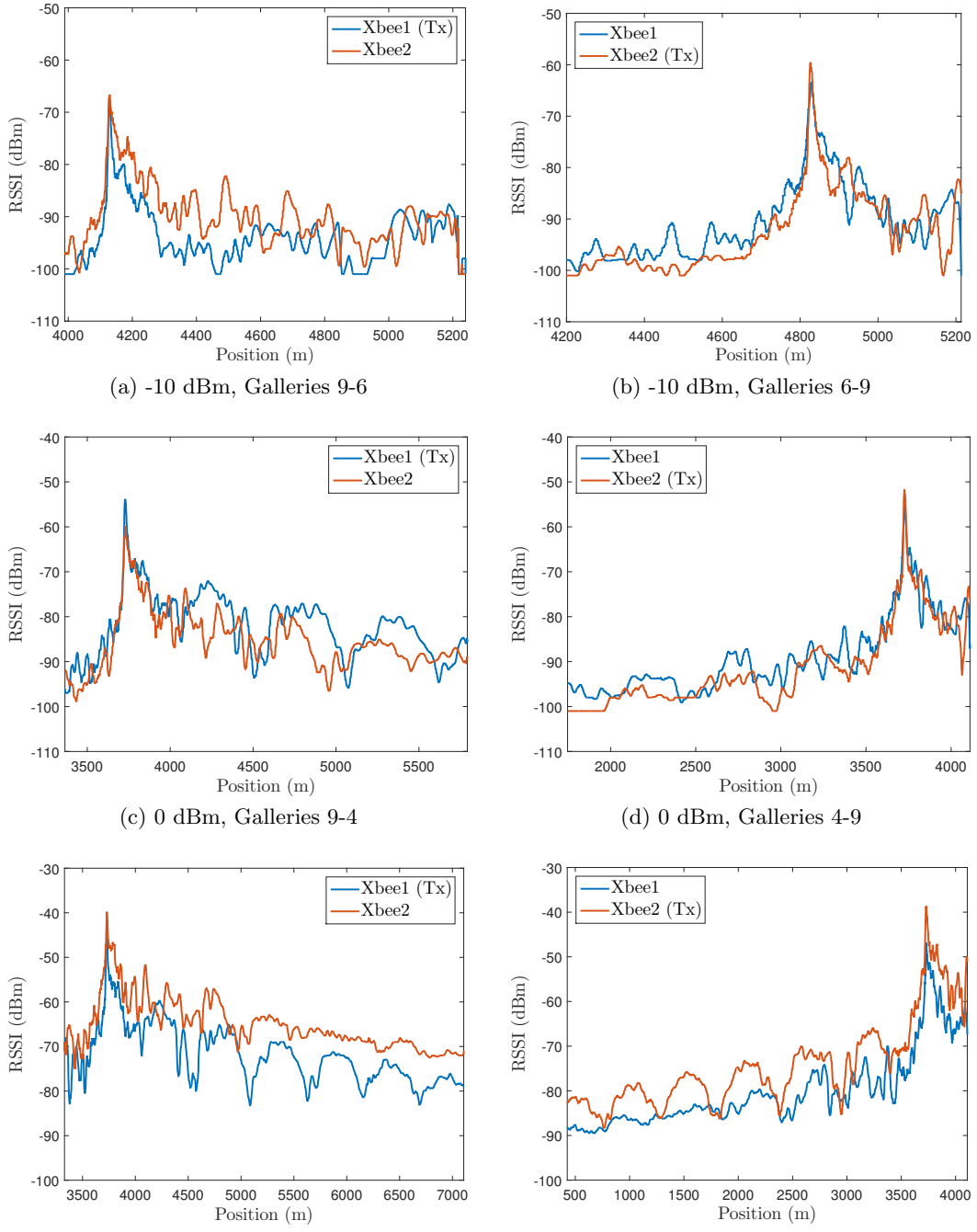

(a) -10 dBm, Galleries 9-6

(b) -10 dBm, Galleries 6-9

(c) 0 dBm, Galleries 9-4

(d) 0 dBm, Galleries 4-9

(e) 18 dBm, Galleries 9-1

(f) 18 dBm, Galleries 1-9

Figure A.1: Fadings measured during the experiment. The closest module to the sending side is indicated by (Tx).

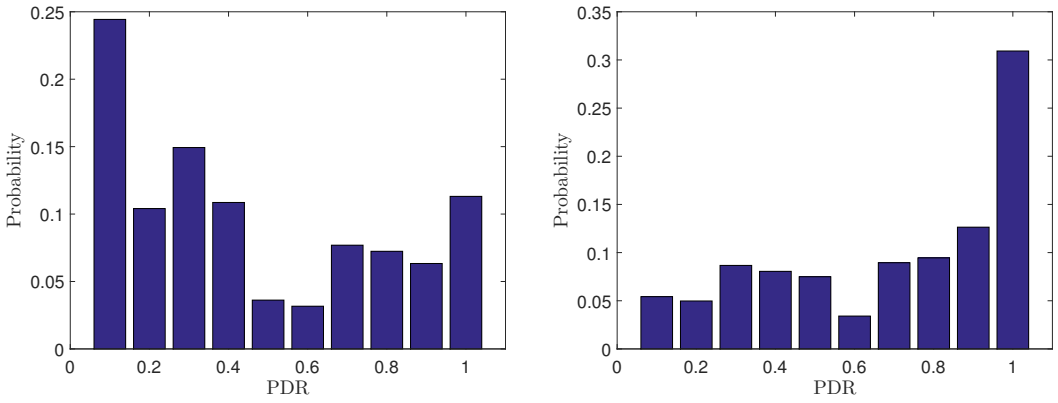

(a) [-105, -100) dBm

(b) [-100, -95) dBm

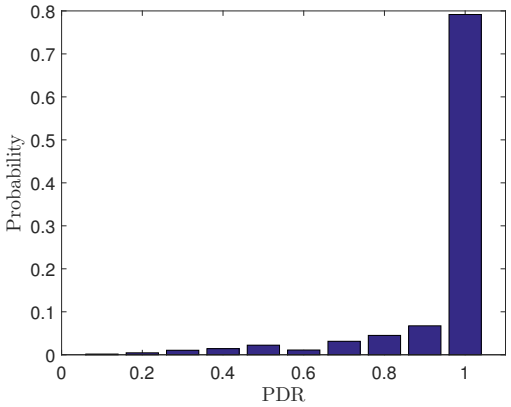

(c) [-95, -90) dBm

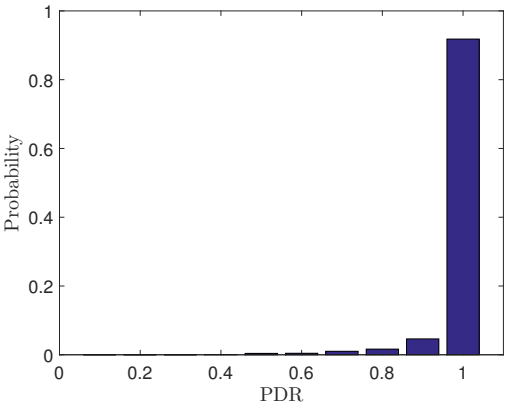

(d) [-90, -85) dBm

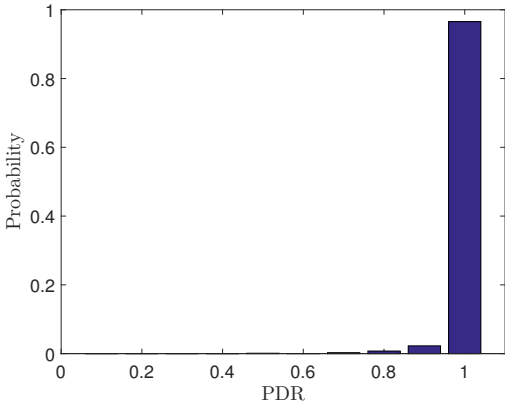

(e) [-85, -80) dBm

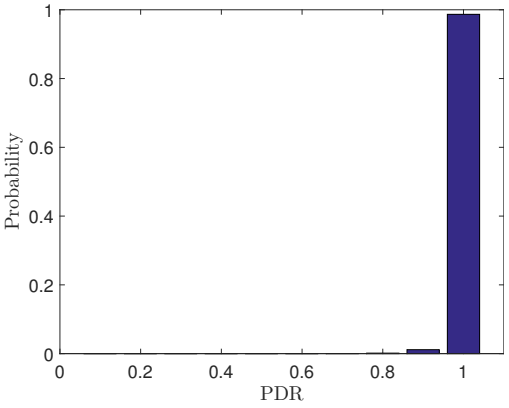

(f) [-80, -75 dBm)

Figure A.2: Distribution of the PDR for different RSSI ranges.

Appendix B

Article: *Low-Bandwidth Telerobotics in Fading Scenarios*

Low-Bandwidth Telerobotics in Fading Scenarios

S. Barrios[1], N. Ayuso[1], D. Tardioli[2], L. Riazuelo[1],
A.R. Mosteo[2], F. Lera[1], and J.L. Villarroel[1]

[1] Aragón Institute for Engineering Research (I3A)
University of Zaragoza
Zaragoza, Spain
{666180, nayuso, riazuelo, lera, jlvilla}@unizar.es
[2] Aragón Institute for Engineering Research (I3A)
Centro Universitario de la Defensa
Zaragoza, Spain
{dantard, amosteo}@unizar.es

Abstract. Sensor networks can monitor wide areas to gather information and relay alerts about concerning events. Response robotic missions in confined scenarios where such a network existed, like tunnels or mines, could take advantage of it as a backbone. This paper addresses challenges arising from the combined characteristics of nodes, typically of low power and bandwidth, and signal propagation in such scenarios, that exhibits extended range but also blind spots due to waveguide self-interference. Firstly, a measurement campaign is reported that characterized RSSI and PDR performance of XBee nodes in the Somport tunnel, enabling improved placement of nodes. Then, a teleoperation mission is demonstrated in which a mobile robot that relays rangefinder readings is commanded thought a backbone multi-hop network, within the restrictions of the extremely limited bandwidth of the IEEE 802.15.4 protocol.

1 Introduction

Sensor based networks have registered a constant growth in the last 20 years. The use of battery-powered nodes with communication capabilities has simplified the surveying of not easily accessible or dangerous environments. This includes mines, nuclear plants or tunnels where the access of human beings can be sometimes harmful as, for example, in case of fire or gas leaks. The deployment of low-power wireless nodes allows to monitor this type of scenarios without the need to install long and expensive cables, with a battery life of months or even years. In this way, the information collected by the nodes is sent to a so-called sink node that acts as an aggregator and can be connected to the wired network and, possibly, to the Internet. The data can be checked remotely but sometimes it can be useful to have the possibility of checking the situation on site especially if the readings provided by the sensors show some unexpected or worrying value.

This can be made using a mobile robot that can be teleoperated taking advantage of the pre-existing sensors' infrastructure that would be in charge of

routing teleoperation-related information from the robot to the operator (possibly through the Internet).

However, on the one hand, the bandwidth offered by such small devices is extremely limited especially if the communication is required to be multi-hop and, on the other hand, the propagation in this kind of confined environments has substantially different characteristics than in open space. Specifically, as has been studied in [1], in the ultra high frequency band (300-3000 MHz) the wireless transmission along tunnel-like environments takes the form of waveguide propagation. This allows the communication over a range of several kilometers thanks to the reduced attenuation per unit length but favouring the appearance of fadings, periodic zones where the signal strength is weaker.

These characteristics pose two different challenges: 1) the positioning of the nodes must be based on a criterium other than the simple distance among peers and 2) it is necessary to reduce the amount of data needed for teleoperation.

The contribution of this paper is twofold. On the one hand, we provide a method to position a set of sensor nodes along a long tunnel taking into account the characteristics of the propagation inside the tunnel itself and verifying the results with a measuring campaign. On the other hand, we propose a scheme to teleoperate a robot along the tunnel using the extremely reduced bandwidth available and demonstrate this achievement with a real-world experiment.

The remainder of this paper is organized as follows. In Section 2 the related works are presented. Section 3 describes the propagation of the communication signal in tunnels as well as a nodes deployment based on experimental analysis. Section 4 addresses the teleoperation issue, dealing with bandwidth limitations. In Section 5 we develop a proof of concept experiment in which we set up a robot teleoperation. Finally, conclusions form Section 6.

2 Related work

Prior research on robots and wireless sensor-network interactions has not considered the use of preexisting communication infrastructure for the mobile robot teleoperation in fading scenarios, to the best of our knowledge.

Dunbabin *et. al* presented an Autonomous Underwater Vehicle (UAV) vision based navigation, able to collect data from many static Underwater Sensor Nodes (USN) networked together optically and acoustically [2]. Palmer *et. al* considered USN with depth adjustment capabilities that allow IEEE 802.15.4 communication between surface nodes as well as between a node and the UAV remotely controlled with an additional 802.15.4 radio [3].

Teleoperation of Unmanned Ground Vehicles (UGVs) in harsh environments through the wireless LAN has been studied, facing the inherent problems due to the propagation characteristics in such environments. The performance and stability of even the simplest teleoperation systems involving vehicles mounted cameras' video feeds and hand controlled motion commands can be committed. Shim and Ro faced the problem of random and unbounded communication time delay [4]. This work proposed measuring the round trip time (RTT) on real-time

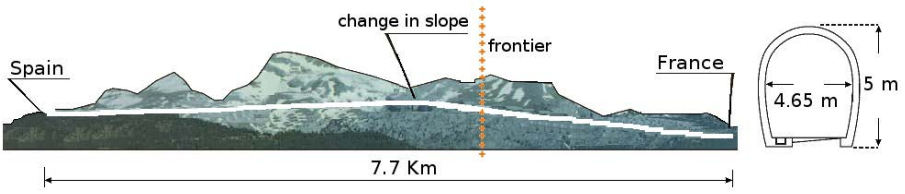

Fig. 1: The somport tunnel.

to switch the best control mode. In [5], the radio signal strength (RSS) gradient at the UGV location has been graphically represented for naturally guiding the human operators to drive the mobile robot (UGV) for reliable communications. In [6] the authors propose a complete system for tunnel intervention where a team of robots is teleoperated over a multi-hop network. Finally, because of the intrinsic bandwidth fluctuations, Gomes *et. at*, proposed an approach based on ROS (Robot Operating Systems) that increases the operators overall performance in low bandwidth situations by strategies to optimize all displayed information transmission quality [7].

3 Signal Propagation and Nodes Deployment

Wireless communication systems have become increasingly important as they represent, most of the time, a faster, more economical, and sometimes the only option to deploy a network, as in the case involving mobile agents. A huge effort has been made in terms of mathematical modeling and measuring campaigns in order to predict radio-wave propagation in different types of scenarios, from indoor, outdoor, urban to even underground, with the final goal of ensuring a good quality communication link and to increase the channel capacity. Among these scenarios, tunnels have attracted the attention for train applications, vehicular networks, and even service and surveillance missions in both military and civilian context [8–11]. Wireless propagation in these environments is described as strongly multipath, and if the wavelenght of the signal is much smaller than the tunnel cross section they act as an oversized dielectric waveguide, extending the communication range but affecting the signal with strong fadings [1, 12].

The analysis of electromagnetic waves propagation inside a tunnel with arbitrary cross section is not analytically feasible. Even for simple geometries, such as rectangular or circular cross sections, no exact closed form solutions are available. To obtain approximate solutions, the most common approaches are the Modal Theory, which takes into consideration the interaction between the propagating modes [13, 14] and the Geometrical Optics Theory (such as the Ray Tracing approach), which models radio signals as rays [15, 16]. For these reasons, we proceed to analyze experimentally the signal propagation in a specific environment: the Somport Railway Tunnel. Based on the propagation already analyzed in [17, 18], the objective is to characterize the communication link, finding a distance between nodes which allows ensuring a correct operation of the network. In this way, the experiment focuses on two measurements. First, the

(a) XBee 802.15.4 (b) XBee-Pro 802.15.4 (c) XBIB-U-DEV

Fig. 2: RF modules (a, b) and USB interface board (c).

RSSI (Received Signal Strength Indicator) along the tunnel, obtaining the maximum communication range for different emission powers as well as the location of the fadings. Second, the RSSI - PDR (Packet Delivery Ratio) relationship, obtaining the minimum RSSI that guarantees the correct reception of the information exchanged between nodes. Finally, by joining both measurements, a deployment strategy is proposed.

3.1 The Somport Railway Tunnel

The Somport Railway Tunnel is the location chosen to perform the experiment. It is an out-of-service tunnel which connects Spain and France through the Pyrenees.

It is 7.7 km long and has a horseshoe-shaped section, approximately 5 m high and 4.65 m wide (Fig. 1). The tunnel is straight along its entire length, suffering a change in slope at approximately 4 km from the Spanish entrance. The walls are limestone with short sections covered with a thin concrete layer. Thanks to its characteristics, it is an ideal environment to perform experiments and emulate long tunnels, common in transport or mining applications.

3.2 Measurement Setup

As previously mentioned, the behavior of the tunnel as waveguide depends on the wavelength being much smaller than the transverse dimension of the tunnel. In other words, the higher the signal frequency, the lower the attenuation factor per unit length, disregarding wall roughness effects. An experimental analysis of the signals propagation in different frequencies of the ISM band (Industrial, Scientific and Medical) is performed in [17]. As a result, it is determined that the 2.4 GHz and 5.2 GHz signals have a much lower attenuation factor than those of 433 MHz and 868 MHz. For this reason, 2.4 GHz is the selected frequency band, since it has a high propagation range, a reasonable wall roughness tolerance and a wide variety of hardware available on the market.

Regarding the communications protocol, since one of the objectives of this work is the development of a low energy consumption wireless sensor network (WSN), IEEE 802.15.4 is the chosen one [19]. This technical standard specifies the physical and media access control layers for LR-WPANs (Low-Rate Wireless

(a) Instrumented vehicle (b) Emitter module

Fig. 3: Receiver modules on mobile platform (a) and emitter module setup (b).

Personal Area Networks). It is suitable for communication in networks with low cost devices and low transfer rates, up to 250 kbit/s. In this way, and in exchange for a lower bandwidth, it allows a much lower power consumption than other standards such as IEEE 802.11 [20], maximizing the battery life of each node.

According to the specifications described, the chosen RF (radio frequency) modules are Digi's XBee 802.15.4 (Fig. 2a) and XBee-Pro 802.15.4 (Fig. 2b), due to their flexibility and low cost. These devices communicate over IEEE 802.15.4, emitting in a power range of -10 to 0 dBm and 10 to 18 dBm, respectively. They allow a maximum payload of 100 bytes, even tough the maximum size of the 802.15.4 MAC frame is limited to 127 bytes. In addition, they are mounted on XBIB-U-DEV interface boards (Fig. 2c), allowing the connection to a computer via USB. Concerning the antennas, Fig. 2 shows 2 different types depending on the module: XBee 802.15.4 uses a whip antenna with a gain of 1.5 dBi. On the other hand, the XBee-Pro 802.15.4 has a 2.1 dBi dipole antenna.

Regarding the location of the devices, the emitter (Tx) module is placed on a 180 cm tripod separated 160 cm from the wall (Fig. 3b). This position is chosen in order to produce better defined and predictable fadings, as [21] reports. In order to avoid the effect of the change in slope, the emitter is placed close to the highest point of the tunnel, at approximately 4 km from the Spanish entrance (Fig. 1).

The selected emission powers are -10, 0 and 18 dBm. The Tx module broadcasts packets of 60 bytes with a numeric identifier, which are captured by an array of two XBee-Pro 802.15.4 modules, allowing to characterize the influence of transversal fadings. The array modules have a sensitivity of -100 dBm and are at 200 cm height and separated 120 cm apart. As in [22] and [21], the spacing between two successive modules is fixed to be greater than one half of the wavelength, so that the coupling between antennas is minimized.

The receiver array is moved along the tunnel using an off-road vehicle as mobile platform (Fig. 3a). In order to synchronize the received packets with the position in the tunnel, it is equipped with two 0.5 degree resolution encoders and a Scanning Laser Rangefinder. The vehicle localizes itself along the tunnel using

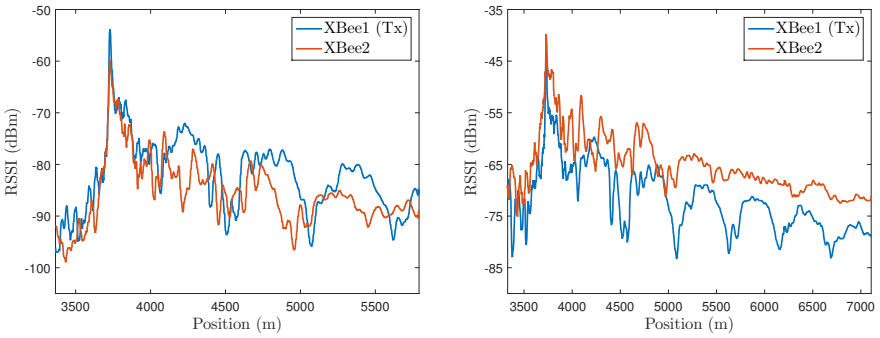

(a) 0 dBm, Galleries 9-4 (b) 18 dBm, Galleries 9-1

Fig. 4: RSSI measured during the experiment. The closest module to the sending side is indicated by (Tx).

a localization algorithm on a previously built map [23], allowing to maintain the same position reference for all the experiments.

The experiment consists of six sweeps along the tunnel. For each emission power of the selected set (-10, 0 and 18 dBm), a route is made from the emitter, moving away until the loss of the signal. At this point, the vehicle returns to the starting point, resulting in two sweeps per power.

3.3 Results of the experiment

First, the signal propagation is analyzed in the regions near the emitter. The packets have been received by the modules, located at the ends of the array (XBee1 and XBee2), differentiating between the closest to the emitter side (Tx) and the furthest one, since it is not placed at the center of the tunnel. Fig. 4 shows the RSSI of the packets collected during the sweeps 3 and 5. The phenomena of the fadings can be appreciated mainly in the signal received by the closest module to the emitter (Fig. 4a). In correspondence with [21], the fadings have a spatial period of about 500 m. Regarding the signal received by the other module, it does not present fadings as sharp as the first one. However, the RSSI level is enough to ensure a suitable communications link (Fig. 4b).

The next step is the measurement of the link quality. The objective is to find a minimum RSSI which allows ensuring the correct communication between two adjacent nodes. The chosen quality estimator is Packet Delivery Ratio (PDR), which is defined as the proportion of number of packets delivered against the number of packets sent. Since it is a global measure and it is necessary to analyze the PDR during the sweep, a moving average of 20 packets is applied in order to obtain its evolution during the path. Thus, the packets received during the whole experiment are grouped in different ranges according to their RSSI. For each range, the percentage of windows with a PDR equal to 1 is found. This gives a measure of how likely it is that all packets reach their destination for a given RSSI range. The results are shown in Table 1. It can be observed that for RSSI values higher than -80 dBm the percentage of windows with a maximum

Table 1: Results of the link quality study.

Range (dBm)	**No. of Packets**	**% PDR = 1**
[-105, -100)	227	11.31
[-100, -95)	1805	30.93
[-95, -90)	5454	79.17
[-90, -85)	5717	91.81
[-85, -80)	5215	96.56
[-80, -75)	4839	98.68
[-75, -70)	4149	98.84
[-70, -65)	3838	98.98
[-65, -60)	1880	99.73
[-60, -55]	975	100

PDR is greater than 98%. Depending on the application, it will be necessary to prioritize a greater reliability of packet delivery or to sacrifice it for a greater range of coverage per node. In this work a 98% probability is considered sufficient, which means that each node receives the packets of the adjacent one with a RSSI higher than -80 dBm. Table 2 shows the maximum range achieved during the experiments meeting the cited minimum RSSI requirement. It can be verified that even for the same power, there are different ranges depending on the module and the path. This is due to the fact that the transverse separation of the receivers to the wall has not been constant during the experiment. Hence, the transversal fadings have a strong influence on the RSSI of the received packets. Therefore, in order to achieve the indicated maximum ranges, a careful positioning of the transverse separation with respect to the emitter must be performed.

Assuming the nodes are placed in the optimal transverse position, the number of devices needed to cover this tunnel (7.7 km) would be 61, 5 and 3, for emission powers of -10, 0 and 18 dBm, respectively. As detailed in following sections, the addition of repeaters reduces the network bandwidth in a factor $(n-1)$, being n the total number of nodes, since there is not spatial reuse. This is not problematic when monitoring the scenario, because the size of the measured data is usually small, as well as the frequency of sensing. However, for a high number of nodes, it implies a difficulty in establishing a continuous communication, as is the teleoperation of a robot.

Hence, there are two different problems with different requirements that must be addressed separately. First, the teleoperation of a robot needs the highest coverage range using the least number of nodes. On the other hand, the monitoring of the scenario requires a higher number of nodes emitting with a low power. For this reason, the use of devices with several different emission levels is proposed. In this way, they can work in low power during a monitoring situation, where there is not high bandwidth requirement. Besides, in an emergency context where the teleoperation of a robot is needed, a minimum number of nodes can raise their power, diminishing the number of hops and providing a higher bandwidth to the network.

Table 2: Maximum distance where a RSSI of -80 dBm is obtained. Underlined measurements are obtained in the modules next to the sending side.

Sweep	Power (dBm)	XBee1 Range (m)	XBee2 Range (m)
1	-10	46	127
2	-10	123	102
3	0	1 557	1013
4	0	379	385
5	18	3 380	3378
6	18	1613	2 780

Besides, it is necessary to consider that the RSSI is not kept above the minimum desired value during the whole path. Due to the phenomenon of fadings, there are areas where the link quality is lower than desired. In this way, forbidden regions are established, where the deployment of a node is not advisable. Fig. 5 shows these zones for emission powers of 0 and 18 dBm. In the case of the greater power, it is observed that the zones coincide with the valleys of the fadings, being periodic and predictable. On the other hand, the smaller powers from these regions in higher areas of the fadings, making them comparable in length with the regions suitable for deployment.

Therefore, a simple deployment strategy consists of placing the node $i+1$ in the coverage range of the node i, avoiding the forbidden regions. Since monitoring applications usually require a periodic separation distance d between sensors, a node position may coincide with a forbidden region. In this case, it would be deployed in the closest previous suitable zone.

4 A proof of concept

In this section, we are going to show the results of a proof of concept experiment in which we set up a robot teleoperation over a backbone network made of XBee

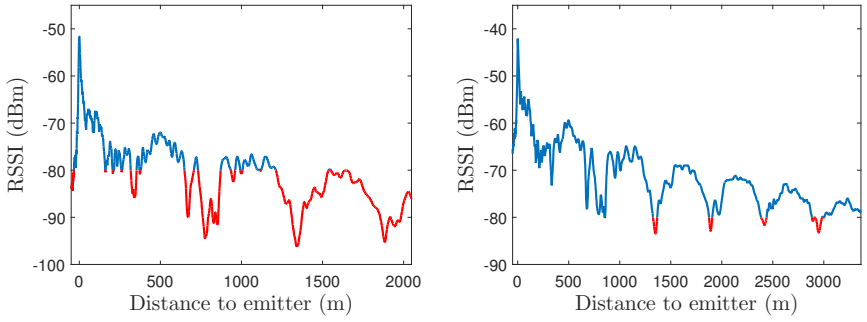

(a) 0 dBm, XBee1 (Tx) (b) 18 dBm, XBee1 (Tx)

Fig. 5: Forbidden regions for the node deployment in the sweeps 3 and 5, respectively. Zones where the RSSI is below the minimum required (-80 dBm) are plotted in red while Tx indicates that the module was the closest to the sending side.

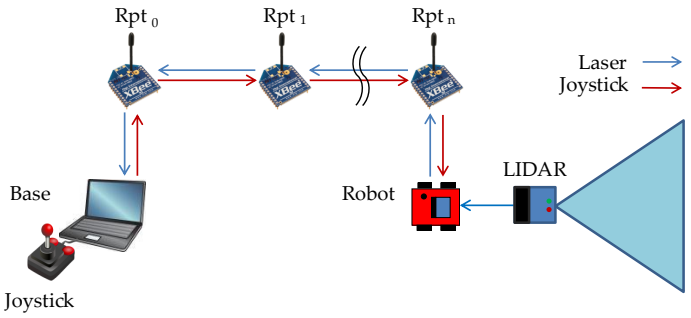

Fig. 6: Teleoperation scheme.

nodes. The goal is to control the movement of a Pioneer P3DX robot using a joystick while receiving LIDAR reading feedback (Fig. 6).

The system is built on top of the ROS (Robotics Operating System) [24] middleware and consists in several nodes connected over the cited network using a multi-core scheme. In Fig. 7 it is possible to observe the conceptual design of the system: the *JOY* node connected with the joystick publishes the stick movements messages through the */joy* topic; it is read by the *TEO_BASE* node that serializes the information (see below) and sends it over the network. On the other side, the messages are received and deserialized by the *TEO_ROBOT* node and published on the */cmd_vel* topic that, in turn, is read by the *ROSARIA* node, which is in charge of sending the velocity commands to the actual robot. In the other direction the LIDAR readings are published by the *SICK* node on the */scan* topic and read by the *TEO_ROBOT* node that, again, serializes the data before sending it over the network. On the base station side, it is deserialized and published in the */comp_scan* node to be shown by the *RVIZ* node. Notice that the nodes on the two ends do not share any *roscore* since each of them consists in a independent ROS system connected through a non-ROS network. Thus, they share in a periodic and asynchronous way the information about the LIDAR and joystick readings.

4.1 Adapting to the available bandwidth

Although the theoretical bandwidth of the XBee modules is 250 kbps, the maximum measured experimentally is only 32.5 kbps, due to the bottleneck that their serial port communication introduce. Additionally, the use of repeaters in a network reduces the raw bandwidth by a factor of $1/(n-1)$, being n the total number of nodes. Considering the case of the Somport tunnel, emitting at the maximum power would require the use of 3 nodes, which would suppose a bandwidth of 16 kbps. On the other hand, in the case of 10 dBm, the resulting bandwidth would be 8 kbps, since 5 nodes would be required. As described, the system is conceptually very simple but being the bandwidth so limited, it has been necessary to reduce the information sent in order to be able to obtain

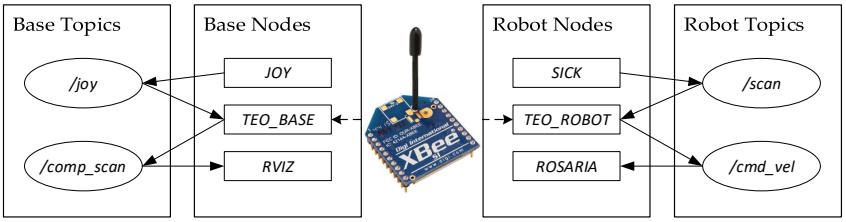

Fig. 7: ROS nodes and topics involved in the system.

an acceptable loop rate. For example, the *SICK* node configured as in our experiment (and connected via serial port to the computer) produces 180 range readings (one per degree) at a frequency of 4Hz. This corresponds, taking also into account the additional data published (timestamp, max and min range, etc.), to approximately 0.8 KB of data, 4 times per second that is, 3.2 KB/s. Since the maximum payload of the XBee modules is 100 bytes, sending the raw data would imply splitting the LIDAR message in at least 8 parts and then merge them at the receiver side to rebuild it. This has two implications: on the one hand sending 8 different messages over a network would take several milliseconds (especially over a multi-hop one) reducing the loop rate. On the other hand, the loss of a single message would mean being unable to reconstruct the information. A similar consideration can be made with the joystick commands, even if in this case the information fits in a single packet. Additionally, the more the bandwidth used for these tasks, the less bandwidth available for others. To mitigate this problem, we decided to *compress* the data as described below.

4.2 Compressing the data

Having high precision and resolution data is usually indicative of a correct system performance. However, if the bandwidth is limited it might not be possible or convenient. Since this is the case, we decided to reduce the information sent to the minimum necessary to find the data themselves useful. To do so, the precision and the resolution of the data is decreased, maintaining a more than acceptable level. Specifically, the ranges representation is reduced from *float64* (8 bytes) to a single byte of information. The length of each reading is thus scaled to 256 possible values and the maximum range is reduced to 4 m independently on the actual range of the LIDAR sensor. All the values above that will be assigned the out-of-range value of *0xFF*. This provides an accuracy of 4 m/254 = 1.5 cm,

Table 3: Packet Delivery Ratio (PDR) and Inter-Arrival Time (IAT) measured during the experiment. Full indicates the percentage of laser packets recomposed using their two halves.

LIDAR				Joystick		
PDR (%)	Full (%)	μ IAT (ms)	σ IAT (ms)	PDR (%)	μ IAT (ms)	σ IAT (ms)
100	76.6	207	80	91	282	105

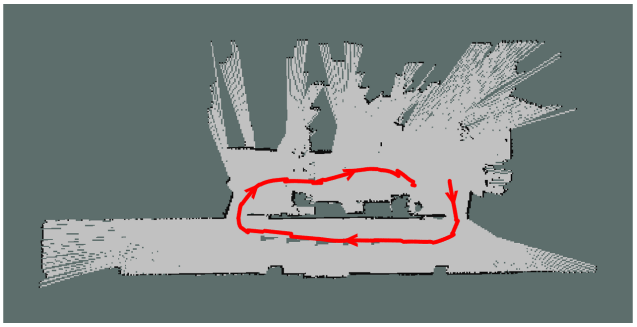

Fig. 8: Results of the teleoperation experiment. The red line indicates the path followed by the robot.

only 0.5 cm worse than that of the Hokuyo URG-04LX, just to give an example, and more that enough for a teleoperation task where the maximum speed of the robot is limited (0.5 m/s in our experiments).

However, even with this reduction, the whole laser scan does not fit in a single packet (we need at least 180 byte, and the maximum payload is 100 bytes), so it is split in 2 halves, using 1 byte as identifier. In order to avoid losing all the information in case one of the two packets does not reach the destination, we send in the first packet the even laser readings (0º, 2º, etc.) and then the uneven. If a message cannot be completed with the second part or only the second part is received, the message is published anyway filling the missing information with the *out-of-range* value. In this way it is possible to have a valuable feedback information also in lossy networks.

5 Real-world testing

In order to demonstrate the correct functioning of the system, the following experiment is proposed. Given a room with two doors communicated externally by a corridor, the goal is to teleoperate the robot, making it exit through one and return by the other using only the visual LIDAR feedback to perform the task. Both the LIDAR and joystick data were sent every 200 ms which is fast enough for an effective teleoperation while this period allows leaving free bandwidth for other possible flows. The information is sent through a network formed by 4 XBee modules. Fig. 8 shows the path achieved, where the map has been generated using a SLAM node running in the robot itself while Table 3 shows the results in terms of inter-arrival time and PDR for each flow. As can be checked, it was possible to teleoperate the Pioneer P3DX, which is 40 cm wide approximately, through a door of comparable size.

6 Conclusions

Wireless sensor networks have allowed in the last 20 years the surveying of hostile or dangerous environments like mines, nuclear plants or tunnels where the access

of human beings can be dangerous as in case of fire or gas leaks. However, the distribution of the nodes in the environment is subject to many factors as communication range, sensing requirements and so on. Also, they are usually static which means that in case of unexpected readings there is no way to know what's actually happening. In this paper we proposed two different contributions. On the one hand, we present a way of positioning a set of sensor nodes in fading environments, like tunnels or mines, taking into account their peculiar propagation pattern and as a function of the transmission power that directly affects the battery life. On the other hand, we propose the use of the sensor nodes as an emergency backbone network to provide network communication to a mobile robot with the end of teleoperating it for on-site intervention in case of unexpected reading or necessity, for example, with the extremely limited bandwidth provided by the 802.15.4 protocol commonly used by sensor networks. The measuring campaign performed allow us to provide parameters that can be useful in similar settings. Additionally, the real-world teleoperation experiment demonstrates that such teleoperation is possible allowing a remote operator to explore the environment with the sole LIDAR feedback.

References

1. A. Emslie and R. Lagace and P. Strong, "Theory of the propagation of UHF radio waves in coal mine tunnels," *IEEE Transactions on Antennas and Propagation*, vol. 23, pp. 192–205, Mar 1975.
2. M. Dunbabin, P. Corke, I. Vasilescu, and D. Rus, "Data Muling over Underwater Wireless Sensor Networks using Autonomous Underwater Vehicle," in *2006 IEEE International Conference on Robotics and Automation*, pp. 2091–2098, May 2015.
3. J. Palmer, N. Yuen, J.-P. Ore, C. Detweiler, and E. Basha, "On Air-to-Water Radio Communication between UAVs and Water Sensor Networks," in *2015 IEEE International Conference on Robotics and Automation*, pp. 5311–5317, July 2015.
4. K. Shim and Y. Ro, "The mobile Robot Teleoperation to consider the stability over the time-delay of wireless network," in *2003 7th Korea-Russia International Symposium*, vol. 2, pp. 457–461, July 2003.
5. S. Caccamo, R. Parasuraman, F. Båberg, and P. Ögren, "Extending a UGV Teleoperation FLC Interface with Wireless Network Connectivity Information," in *2015 IEEE/RSJ International Conference on Intelligent Robots and Systems*, pp. 4305–4312, September 2015.
6. D. Tardioli, D. Sicignano, L. Riazuelo, A. Romeo, J. L. Villarroel, and L. Montano, "Robot teams for intervention in confined and structured environments," *Journal of Field Robotics*, vol. 33, no. 6, pp. 765–801, 2016.
7. J. Gomes, F. Marques, A. Lourenço, R. Mendonça, and J. Barata, "Gaze-Directed Telemetry in High Latency Wireless Communications: The Case of Robot Teleoperation," in *42nd Annual Conference of the IEEE Industrial Electronics Society*, pp. 704–709, December 2016.
8. E. Masson, Y. Cocheril, P. Combeau, L. Aveneau, M. Berbineau, R. Vauzelle, and E. Fayt, "Radio wave propagation in curved rectangular tunnels at 5.8 GHz for metro applications," in *ITS Telecommunications (ITST), 2011 11th International Conference on*, pp. 81–85, IEEE, 2011.

9. L. Bernadó, A. Roma, A. Paier, T. Zemen, N. Czink, J. Karedal, A. Thiel, F. Tufvesson, A. F. Molisch, and C. F. Mecklenbrauker, "In-tunnel vehicular radio channel characterization," in *Vehicular Technology Conference (VTC Spring), 2011 IEEE 73rd*, pp. 1–5, IEEE, 2011.
10. C. Cerasoli, "RF propagation in tunnel environments," in *IEEE MILCOM 2004. Military Communications Conference, 2004.*, vol. 1, pp. 363–369 Vol. 1, Oct 2004.
11. E. Kjeldsen and M. Hopkins, "An experimental look at RF propagation in narrow tunnels," in *Military Communications Conference, 2006. MILCOM 2006. IEEE*, pp. 1–7, IEEE, 2006.
12. P. Delogne, "EM propagation in tunnels," *IEEE Transactions on Antennas and Propagation*, vol. 39, no. 3, pp. 401–406, 1991.
13. S. F. Mahmoud and J. R. Wait, "Guided electromagnetic waves in a curved rectangular mine tunnel," *Radio Science*, vol. 9, no. 5, pp. 567–572, 1974.
14. D. G. Dudley, M. Lienard, S. F. Mahmoud, and P. Degauque, "Wireless propagation in tunnels," *IEEE Antennas and Propagation Magazine*, vol. 49, no. 2, pp. 11–26, 2007.
15. S. F. Mahmoud and J. R. Wait, "Geometrical optical approach for electromagnetic wave propagation in rectangular mine tunnels," *Radio Science*, vol. 9, no. 12, pp. 1147–1158, 1974.
16. S.-H. Chen and S.-K. Jeng, "SBR image approach for radio wave propagation in tunnels with and without traffic," *IEEE Transactions on Vehicular Technology*, vol. 45, no. 3, pp. 570–578, 1996.
17. C. Rizzo and F. Lera and J. L. Villarroel, "UHF and SHF Fading Analysis Using Wavelets in Tunnel Environments," in *2013 IEEE 78th Vehicular Technology Conference (VTC Fall)*, pp. 1–6, Sept 2013.
18. C. Rizzo, F. Lera, and J. L. Villarroel, "Transversal fading analysis in straight tunnels at 2.4 GHz," in *2013 13th International Conference on ITS Telecommunications (ITST)*, pp. 313–318, Nov 2013.
19. IEEE Computer Society, "IEEE Standard for Information Technology - Telecommunications and Information Exchange Between Systems - Local and Metropolitan Area Networks Specific Requirements Part 15.4: Wireless Medium Access Control (MAC) and Physical Layer (PHY) Specifications for Low-Rate Wireless Personal Area Networks (LR-WPANs)," *IEEE Std 802.15.4-2003*, pp. 1–670, October 2003.
20. IEEE Computer Society, "IEEE Standard for Information Technology - Telecommunications and Information Exchange Between Systems - Local and Metropolitan Area Networks - Specific Requirements - Part 11: Wireless LAN Medium Access Control (MAC) and Physical Layer (PHY) Specifications," *IEEE Std 802.11-2007 (Revision of IEEE Std 802.11-1999)*, pp. 1–1076, June 2007.
21. C. Rizzo, J. L. Villarroel and F. Lera, *Propagation, Localization and Navigation in Tunnel-like Environments.* PhD thesis, University of Zaragoza, 2015.
22. Molina-Garcia-Pardo, J.-M. and Lienard, M. and Degauque, P., "Propagation in Tunnels: Experimental Investigations and Channel Modeling in a Wide Frequency Band for MIMO Applications," *EURASIP Journal on Wireless Communications and Networking*, vol. 2009, no. 1, p. 560571, 2009.
23. M. T. Lázaro and J. A. Castellanos, "Localization of probabilistic robot formations in SLAM," in *2010 IEEE International Conference on Robotics and Automation*, pp. 3179–3184, May 2010.
24. Morgan Quigley and Ken Conley and Brian P. Gerkey and Josh Faust and Tully Foote and Jeremy Leibs and Rob Wheeler and Andrew Y. Ng, "ROS: an open-source Robot Operating System," in *ICRA Workshop on Open Source Software*, 2009.

Bibliography

[1] Y. Chen and D. Zhang and J. Chen and K. Liu and F. Yang, "A new fire protection system of power cable tunnel based on wireless sensor network monitoring system," in *2016 IEEE 11th Conference on Industrial Electronics and Applications (ICIEA)*, pp. 1103–1106, June 2016.

[2] M. Ceriotti and M. Corrà and L. D'Orazio and R. Doriguzzi and D. Facchin and S. T. Gună and G. P. Jesi and R. L. Cigno and L. Mottola and A. L. Murphy and M. Pescalli and G. P. Picco and D. Pregnolato and C. Torghele, "Is there light at the ends of the tunnel? Wireless sensor networks for adaptive lighting in road tunnels," in *Proceedings of the 10th ACM/IEEE International Conference on Information Processing in Sensor Networks*, pp. 187–198, April 2011.

[3] IEEE Computer Society, "IEEE Standard for Information Technology - Telecommunications and Information Exchange Between Systems - Local and Metropolitan Area Networks Specific Requirements Part 15.4: Wireless Medium Access Control (MAC) and Physical Layer (PHY) Specifications for Low-Rate Wireless Personal Area Networks (LR-WPANs)," *IEEE Std 802.15.4-2003*, pp. 1–670, October 2003.

[4] P. Tao and L. Xiaoyang, "Hybrid Wireless Communication System Using ZigBee and WiFi Technology in the Coalmine Tunnels," in *2011 Third International Conference on Measuring Technology and Mechatronics Automation*, vol. 2, pp. 340–343, Jan 2011.

[5] A. Hrovat and G. Kandus and T. Javornik, "A Survey of Radio Propagation Modeling for Tunnels," *IEEE Communications Surveys Tutorials*, vol. 16, pp. 658–669, Second 2014.

[6] S. Barrios, N. Ayuso, D. Tardioli, L. Riazuelo, A. R. Mosteo, F. Lera, and J. L. Villarroel, "Low-Bandwidth Telerobotics in Fading Scenarios," in *ROBOT'2017: Third Iberian Robotics Conference*, Springer, 2017.

[7] E. Masson, Y. Cocheril, P. Combeau, L. Aveneau, M. Berbineau, R. Vauzelle, and E. Fayt, "Radio wave propagation in curved rectangular tunnels at 5.8 GHz for

metro applications," in *ITS Telecommunications (ITST), 2011 11th International Conference on*, pp. 81–85, IEEE, 2011.

[8] L. Bernadó, A. Roma, A. Paier, T. Zemen, N. Czink, J. Karedal, A. Thiel, F. Tufvesson, A. F. Molisch, and C. F. Mecklenbrauker, "In-tunnel vehicular radio channel characterization," in *Vehicular Technology Conference (VTC Spring), 2011 IEEE 73rd*, pp. 1–5, IEEE, 2011.

[9] C. Cerasoli, "RF propagation in tunnel environments," in *Military Communications Conference, 2004. MILCOM 2004. 2004 IEEE*, vol. 1, pp. 363–369, IEEE, 2004.

[10] E. Kjeldsen and M. Hopkins, "An experimental look at RF propagation in narrow tunnels," in *Military Communications Conference, 2006. MILCOM 2006. IEEE*, pp. 1–7, IEEE, 2006.

[11] J. Boksiner, C. Chrysanthos, J. Lee, M. Billah, T. Bocskor, D. Barton, and J. Breakall, "Modeling of radiowave propagation in tunnels," in *Military Communications Conference, 2012-milcom 2012*, pp. 1–6, IEEE, 2012.

[12] A. Emslie, R. Lagace, and P. Strong, "Theory of the propagation of UHF radio waves in coal mine tunnels," *IEEE Transactions on Antennas and Propagation*, vol. 23, no. 2, pp. 192–205, 1975.

[13] P. Delogne, "EM propagation in tunnels," *IEEE Transactions on Antennas and Propagation*, vol. 39, no. 3, pp. 401–406, 1991.

[14] S. F. Mahmoud and J. R. Wait, "Guided electromagnetic waves in a curved rectangular mine tunnel," *Radio Science*, vol. 9, no. 5, pp. 567–572, 1974.

[15] J. Chiba, T. Inaba, Y. Kuwamoto, O. Banno, and R. Sato, "Radio communication in tunnels," *IEEE Transactions on microwave theory and techniques*, vol. 26, no. 6, pp. 439–443, 1978.

[16] D. G. Dudley, M. Lienard, S. F. Mahmoud, and P. Degauque, "Wireless propagation in tunnels," *IEEE Antennas and Propagation Magazine*, vol. 49, no. 2, pp. 11–26, 2007.

[17] S. F. Mahmoud and J. R. Wait, "Geometrical optical approach for electromagnetic wave propagation in rectangular mine tunnels," *Radio Science*, vol. 9, no. 12, pp. 1147–1158, 1974.

[18] K. R. Schaubach, N. Davis, and T. S. Rappaport, "A ray tracing method for predicting path loss and delay spread in microcellular environments," in *Vehicular Technology Conference, 1992, IEEE 42nd*, pp. 932–935, IEEE, 1992.

[19] S. Y. Seidel and T. S. Rappaport, "A ray tracing technique to predict path loss and delay spread inside buildings," in *Global Telecommunications Conference, 1992. Conference Record., GLOBECOM'92. Communication for Global Users., IEEE*, pp. 649–653, IEEE, 1992.

[20] W. Honcharenko, H. L. Bertoni, J. L. Dailing, J. Qian, and H. Yee, "Mechanisms governing UHF propagation on single floors in modern office buildings," *IEEE Transactions on Vehicular Technology*, vol. 41, no. 4, pp. 496–504, 1992.

[21] S.-H. Chen and S.-K. Jeng, "SBR image approach for radio wave propagation in tunnels with and without traffic," *IEEE Transactions on Vehicular Technology*, vol. 45, no. 3, pp. 570–578, 1996.

[22] A. Hrovat, G. Kandus, and T. Javornik, "A survey of radio propagation modeling for tunnels," *IEEE Communications Surveys & Tutorials*, vol. 16, no. 2, pp. 658–669, 2014.

[23] Z. Sun and I. F. Akyildiz, "Channel modeling and analysis for wireless networks in underground mines and road tunnels," *IEEE Transactions on communications*, vol. 58, no. 6, 2010.

[24] E. Masson, P. Combeau, M. Berbineau, R. Vauzelle, and Y. Pousset, "Radio wave propagation in arched cross section tunnels-simulations and measurements," *Journal of Communication*, vol. 4, no. 4, pp. 276–283, 2009.

[25] C. Gentile, F. Valoit, and N. Moayeri, "A raytracing model for wireless propagation in tunnels with varying cross section," in *Global Communications Conference (GLOBECOM), 2012 IEEE*, pp. 5027–5032, IEEE, 2012.

[26] K. D. Laakmann and W. H. Steier, "Waveguides: characteristic modes of hollow rectangular dielectric waveguides," *Applied Optics*, vol. 15, no. 5, pp. 1334–1340, 1976.

[27] D. M. Pozar, "Microwave Engineering 3e," *Tramsmission Lines and Waveguides*, pp. 143–149, 2005.

[28] J. Molina-Garcia-Pardo, M. Lienard, A. Nasr, and P. Degauque, "On the possibility of interpreting field variations and polarization in arched tunnels using a model for propagation in rectangular or circular tunnels," *IEEE Transactions on Antennas and Propagation*, vol. 56, no. 4, pp. 1206–1211, 2008.

[29] C. Rizzo, J. L. Villarroel and F. Lera, *Propagation, Localization and Navigation in Tunnel-like Environments.* PhD thesis, University of Zaragoza, 2015.

[30] C. Rizzo and F. Lera and J. L. Villarroel, "UHF and SHF Fading Analysis Using Wavelets in Tunnel Environments," in *2013 IEEE 78th Vehicular Technology Conference (VTC Fall)*, pp. 1–6, Sept 2013.

[31] IEEE Computer Society, "IEEE Standard for Information Technology - Telecommunications and Information Exchange Between Systems - Local and Metropolitan Area Networks - Specific Requirements - Part 11: Wireless LAN Medium Access Control (MAC) and Physical Layer (PHY) Specifications," *IEEE Std 802.11-2007 (Revision of IEEE Std 802.11-1999)*, pp. 1–1076, June 2007.

[32] Morgan Quigley and Ken Conley and Brian P. Gerkey and Josh Faust and Tully Foote and Jeremy Leibs and Rob Wheeler and Andrew Y. Ng, "ROS: an open-source Robot Operating System," in *ICRA Workshop on Open Source Software*, 2009.

[33] Molina-Garcia-Pardo, J.-M. and Lienard, M. and Degauque, P., "Propagation in Tunnels: Experimental Investigations and Channel Modeling in a Wide Frequency Band for MIMO Applications," *EURASIP Journal on Wireless Communications and Networking*, vol. 2009, no. 1, p. 560571, 2009.

[34] M. T. Lázaro and J. A. Castellanos, "Localization of probabilistic robot formations in SLAM," in *2010 IEEE International Conference on Robotics and Automation*, pp. 3179–3184, May 2010.

[35] B. Sundararaman, U. Buy, and A. D. Kshemkalyani, "Clock synchronization for wireless sensor networks: a survey," *Ad hoc networks*, vol. 3, no. 3, pp. 281–323, 2005.

[36] J. Elson, L. Girod, and D. Estrin, "Fine-grained network time synchronization using reference broadcasts," *ACM SIGOPS Operating Systems Review*, vol. 36, no. SI, pp. 147–163, 2002.

[37] H. Kopetz and W. Schwabl, *Global time in distributed real-time systems*. Inst. für Techn. Informatik, Univ., 1989.

[38] M. Maróti, B. Kusy, G. Simon, and Á. Lédeczi, "The flooding time synchronization protocol," in *Proceedings of the 2nd international conference on Embedded networked sensor systems*, pp. 39–49, ACM, 2004.

[39] T. M. Schmidl and D. C. Cox, "Robust frequency and timing synchronization for ofdm," *IEEE Transactions on Communications*, vol. 45, pp. 1613–1621, Dec 1997.

[40] D. L. Mills, "Internet time synchronization: the network time protocol," *IEEE Transactions on communications*, vol. 39, no. 10, pp. 1482–1493, 1991.

[41] S. Ganeriwal, R. Kumar, and M. B. Srivastava, "Timing-sync protocol for sensor networks," in *Proceedings of the 1st international conference on Embedded networked sensor systems*, pp. 138–149, ACM, 2003.

[42] W. Ye, J. Heidemann, and D. Estrin, "An energy-efficient MAC protocol for wireless sensor networks," in *INFOCOM 2002. Twenty-First Annual Joint Conference of the IEEE Computer and Communications Societies. Proceedings. IEEE*, vol. 3, pp. 1567–1576, IEEE, 2002.